1 **Comprehensive multi-omics study of the molecular perturbations**

2 **induced by simulated diabetes on coronary artery endothelial cells**

3

4 **Aldo Moreno-Ulloa**[1,2]*, **Hilda Carolina Delgado-De la Herrán**[1,3], **Carolina Álvarez-Delgado**[3],

5 **Omar Mendoza-Porras**[4], **Rommel A. Carballo-Castañeda**[1] **and Francisco Villarreal**[5,6]

6

7 [1]MS2 laboratory, Biomedical Innovation Department, Center for Scientific Research and Higher
8 Education of Ensenada (CICESE), Baja California, México
9 [2]Specialized Laboratory in Metabolomics and Proteomics (MetPro), CICESE, México
10 [3]Mitochondrial Biology Laboratory, Biomedical Innovation Department, Center for Scientific
11 Research and Higher Education of Ensenada (CICESE), Baja California, México
12 [4]CSIRO Livestock and Aquaculture, Queensland Bioscience Precinct, 306 Carmody Rd, St
13 Lucia, QLD, Australia
14 [5]School of Medicine, University of California, San Diego, CA, USA
15 [6]San Diego VA Healthcare System
16

17

18

19 * To whom correspondence should be addressed: Biomedical Innovation Department, CICESE
20 Carretera Ensenada-Tijuana No. 3918, Zona Playitas, CP. 22860, Ensenada, B.C. Mexico,
21 Phone: +52(646)175-05-00 ext. 2721, E-mail: amoreno@cicese.mx

22

23

24

Abstract

Coronary artery endothelial cells (CAEC) exert an important role in the development of cardiovascular disease. Dysfunction of CAEC is associated with cardiovascular disease in subjects with type 2 diabetes mellitus (T2DM). However, comprehensive studies of the effects that a diabetic environment exerts on this cellular type scarce. The present study characterized the molecular perturbations occurring on cultured bovine CAEC subjected to a prolonged diabetic environment (high glucose [HG] and high insulin [HI]). Changes at the metabolite and peptide level were assessed by untargeted metabolomics and chemoinformatics, and the results were integrated with proteomics data using published SWATH-based proteomics on the same *in vitro* model. Our findings were consistent with reports on other endothelial cell types, but also identified novel signatures of DNA/RNA, aminoacid, peptide, and lipid metabolism in cells under a diabetic environment. Manual data inspection revealed disturbances on tryptophan catabolism and biosynthesis of phenylalanine-based, glutathione-based, and proline-based peptide metabolites. Fluorescence microscopy detected an increase in binucleation in cells under treatment that also occurred when human CAEC were used. This multi-omics study identified particular molecular perturbations in an induced diabetic environment that could help unravel the mechanisms underlying the development of cardiovascular disease in subjects with T2DM.

Keywords: SWATH-Proteomics; Metabolomics; Type 2 Diabetes Mellitus; Endothelial cells; Feature-Based Molecular Networking

1. Introduction

Damage to coronary artery endothelial cells (CAEC) leads to coronary endothelial dysfunction, which is associated with the development of cardiac pathologies in subjects with and without coronary atherosclerosis (1). Subjects with type 2 diabetes mellitus (T2DM) are particularly at increased risk of myocardial infarction (2) and coronary endothelial dysfunction has been implicated in the prognosis (3). A high-glucose (HG) environment —hallmark of T2DM— leads to nitric oxide signaling, cell cycle (4), apoptosis (5), angiogenesis (6), and DNA structure impairment (7). However, given the intrinsic heterogeneity of the endothelium, the molecular perturbations caused by HG vary accordingly with the type of studied endothelial cells (8, 9). For instance, human microvascular endothelial cells showed increased gene expression of endothelial nitric oxide synthase, superoxide dismutase 1, glutathione peroxidase 1, thioredoxin reductase 1 and 2 compared to the regulation observed in human umbilical vein endothelial cells (HUVEC) when cultured in HG for 24 h. Furthermore, the response of endothelial cells to HG is influenced by the duration of exposure (10, 11) as demonstrated in bovine aortic and human microvascular endothelial cells where cell proliferation and apoptosis were higher at <48 h compared to 8 weeks of exposure (10). In another example of time-dependent response, increased apoptosis (derived from DNA fragmentation) and tumor necrosis factor alpha protein levels were reported in human coronary artery endothelial cells (HCAEC) after only 24 h of incubation with HG (5). Hence, the molecular response to HG cannot be generalized among endothelial cell types. Previously we reported impaired mitochondrial function/structure and nitric oxide signaling in HG treated HCAEC for 48 h (12). However, a 72 h study documented an increased in pro-inflammatory cytokines (13) and oxidative stress in HCAEC (14). The long-term (>72 h) effect of HG in CAEC has not been as extensively documented compared to other endothelial cell types. Characterizing the effect of HG on CAEC may allow us to identify key signaling pathways (or specific biomolecules) associated with the development of endothelial dysfunction and cardiac pathologies.

Here, liquid chromatography coupled to mass spectrometry (LC-MS^2)-based untargeted metabolomics and SWATH-based quantitative proteomics data, as well as bio- and chemo-informatics were used to characterize the molecular perturbations occurring in Bovine Coronary Artery Endothelial Cells (BCAEC) under a prolonged diabetic environment.

2. Methods

2.1 Chemical and reagents

Recombinant human insulin was purchased from Sigma Aldrich (St. Louis, MO, USA). Antibiotic-antimitotic solution, trypsin-EDTA solution 0.25%, Hank's Balanced Salt Solution (HBSS) without

83 phenol red, Dulbecco's Modified Eagle's Media (DMEM) with glutamine, Fetal Bovine Serum

84 (FBS), Hoechst 33258, Pentahydrate (bis-Benzimide)-FluoroPure™, and methanol-free

85 formaldehyde (16% solution) were obtained from Thermo Fisher Scientific (Waltham, MA, USA).

86 Methanol, Acetonitrile, and water were Optima™ LC-MS Grade and obtained from Fisher

87 Scientific (Hampton, NH, USA). Ethanol LiChrosolv® Grade was obtained from Merck KGaA

88 (Darmstadt, Germany). Rabbit anti-Von Willebrand factor (vWf) antibody and goat anti-rabbit IgG

89 conjugated to Alexa Fluor 488 were obtained from Abcam (Cambridge, MA, USA).

90

91 **2.2 Cell culture**

92 BCAEC were purchased from Cell applications, Inc. (San Diego, CA, USA) and grown as

93 previously described (15). In brief, cells were grown with DMEM (5.5 mmol/L glucose,

94 supplemented with 10% FBS and 1% antibiotic-antimitotic solution) at 37 ^{o}C in an incubator with

95 a humidified atmosphere of 5 % CO_2. Before experiments, cells were switched to DMEM with 1%

96 FBS for 12 h to maintain the cells under a quiescent state. The model to simulate diabetes is

97 described in (15) (**Figure 1**). Endothelial cells were cultured for 12 days to determine the chronic

98 molecular perturbations caused by simulated diabetes and to avoid the early (within 48 h) cell

99 proliferation effects caused by HG (10, 16). In brief, cells were first treated with 100 nmol/L insulin

100 (high-insulin, HI) in normal glucose (NG, 5.5 mmol/L in DMEM) for 3 days (17) and then

101 maintained in high-glucose (HG, 20 mmol/L in DMEM) and constant HI for 9 days. This sequential

102 scheme tried to mimic the pathophysiological conditions that occur in T2DM patients, wherein

103 hyperinsulinemia precedes hyperglycemia (18). Cells were used at passages between 6 to 12.

104 The control group did not receive HI nor HG treatment. For selected experiments (binucleation

105 analysis), HCAEC (55 years old Caucasian male, history of T2DM for >5 years) were purchased

106 from Cell Applications, Inc. and subjected to the same conditions as BCAEC but using MesoEndo

107 Growth Medium (Cell Applications, Inc.) to induce proliferation. For simulated diabetes, HCAEC

108 were treated with HI and HG as with BCAEC but, MesoEndo Growht Medium was used instead.

109 For consistency, the group that underwent simulated diabetes (HG + HI) will be referred to as the

110 "experimental group". All experiments were carried out in triplicate.

111

112 **2.3 Immunofluorescence**

113 As previously described (15), 100,000 cells per well were seeded onto 12-well plates (Corning®

114 CellBIND®) and exposed to simulated diabetes. Thereafter, BCAEC and HCAEC were washed

115 with PBS to remove dead cells and debris. Cells were fixed, permeabilized, and blocked as

116 described before (19). Cells were then incubated with a polyclonal antibody against the vWf

4

117   (1:400, 3% BSA in PBS) overnight at 4°C and thereafter washed 3x with PBS. Alexa Fluor 488-

118   labeled anti-rabbit (1:400 in PBS) was then used as a secondary antibody for 1 h at RT and

119   washed 3x with PBS. As a negative control, cells were incubated only with secondary antibody to

120   assess for non-specific binding. Cell nuclei were stained with Hoechst 33258 (2 µg/ml in HBSS)

121   for 30 min and washed 3x with PBS. Fluorescent images were taken in at least three random

122   fields per condition using an EVOS$^®$ FLoid$^®$ Cell Imaging Station with a fixed 20x air objective.

123   Image analysis was performed through ImageJ software (version 2.0.0).

124

125   **2.4 Metabolite extraction**

126   Cells were seeded at 300,000 cells per well in 6-well plates (Corning$^®$ CellBIND$^®$) and treated as

127   above. After HG and HI conditions, metabolites were extracted following a published protocol for

128   adherent cells with some modifications (20) (**Figure 1**). In brief, after washing the cells 3 x with

129   PBS, 500 µL of a cold mixture of methanol: ethanol (50:50, v:v) were added to each well, covered

130   with aluminum foil, and incubated at -80^{0}C for 4 h. Cells were then scrapped using a lifter (Fisher

131   Scientific, Hampton, NH, USA), and the supernatant was transferred to Eppendorf tubes before

132   centrifugation for 10 min at 14,000 rpm at 4^{0}C. The supernatant was transferred to another tube

133   and dried down by SpeedVac™ System (Thermo Fisher Scientific, Waltham, MA, USA). Samples

134   were reconstituted in water/acetonitrile 95:5 v/v with 0.1% formic, centrifuged at 14,000 rpm for

135   10 min at 4° C. The particle free supernatant was recovered for further LC-MS^2 analysis.

136

137   **2.5 LC-MS^2 data acquisition for metabolomics**

138   Metabolites were loaded into an Eksigent nanoLC$^®$ 400 system (AB Sciex, Foster City, CA, USA)

139   with a HALO Phenyl-Hexyl column (0.5 x 50 mm, 2.7 µm, 90 Å pore size, Eksigent AB Sciex,

140   Foster City, CA, USA) for data acquisition using the LC-MS parameters previously described with

141   some modifications (21). In brief, the separation of metabolites was performed using gradient

142   elution with 0.1% formic acid in water (A) and 0.1% formic acid in ACN (B) as mobile phases at a

143   constant flow rate of 5 µL/min. The gradient started with 5% B for 1 min followed by a stepped

144   increase to 100%, B over 26 min and held constant for 4 min. Solvent composition was returned

145   to 5% B for 0.1 min. Column re-equilibration was carried out with 5% mobile phase B for 4 minutes.

146   Potential carryover was minimized with a blank run (1 µL buffer A) between sample experimental

147   samples. The eluate from the LC was delivered directly to the TurboV source of a TripleTOF

148   5600+ mass spectrometer (AB Sciex, Foster City, CA, USA) using electrospray ionization (ESI)

149   under positive mode. ESI source conditions were set as follows: IonSpray Voltage Floating, 5500

150   V; Source temperature, 350°C; Curtain gas, 20 psi; Ion source gases 1 and 2 were set to 40 and

151   45 psi; Declustering potential, 100 V. Data was acquired using information-dependent acquisition

152   (IDA) with high sensitivity mode selected, automatically switching between full-scan MS and

153   MS/MS. The accumulation time for TOF MS was 0.25 s/spectra over the *m/z* range 100-1500 Da

154   and for MS/MS scan was 0.05 s/spectra over the *m/z* 50-1500 Da. The IDA settings were as

155   follows charge state +1 to +2, intensity 125 cps, exclude isotopes within 6 Da, mass tolerance 50

156   mDa, and a maximum number of candidate ions 20. Under IDA settings, the ''exclude former

157   target ions'' was set as 15 s after two occurrences and ''dynamic background subtract'' was

158   selected. Manufacturer rolling collision energy (CE) option was used based on the size and

159   charge of the precursor ion using formula CE=*m/z* x 0.0575 + 9. The instrument was automatically

160   calibrated by the batch mode using appropriate positive TOF MS and MS/MS calibration solutions

161   before sample injection and after injection of two samples (<3.5 working hours) to ensure a mass

162   accuracy of <5 ppm for both MS and MS/MS data. Instrument performance was monitored during

163   data acquisition by including QC samples (pooled samples of equal volume) every 4 experimental

164   samples. Data acquisition of experimental samples was also randomized.

165

166   **2.6 Metabolomics data processing**

167   Mass detection, chromatogram building and deconvolution, isotopic assignment, feature

168   alignment, and gap-filling (to detect features missed during the initial alignment) from LC-MS^2

169   datasets was performed using XCMS (https://xcmsonline.scripps.edu) (22) and MZmine (23)

170   software. The XCMS pipeline was used for normalization of feature area and statistical analysis.

171   To identify or annotate the metabolites at the chemical structure and class level, the MS^2-

172   containing features extracted with MZmine were further analyzed using the Global Natural

173   Products Social Molecular Networking (GNPS) (24), Network Annotation Propagation (NAP) (25)

174   and MS2LDA (26) *in silico* annotation tools, and Classyfire automated chemical classification (27),

175   as previously described (21) with some modifications. The confidences of such annotations are

176   level 2 (probable structure by library spectrum match) and level 3 (tentative candidates) in

177   agreement with the Metabolomics Standards Initiative (MSI) classification (28). Molecular

178   networking, NAP, and Classyfire outputs were integrated using the MolNetEnhancer workflow

179   (29). Molecular networks were visualized using Cytoscape version 3.8.2 (30). In addition,

180   chemical substructures (co-occurring fragments and neutral losses referred to as "mass2motifs"

181   [M2M]) were recognized using the MS2LDA web pipeline (http://www.ms2lda.org) to further

182   annotate metabolites (level 3, MSI). The detailed processing parameters for XCMS and MZmine

183   pipelines are found in the supporting information.

184

2.7 Peptidomics data processing

For peptide identification, raw .wiff and .wiff.scan files (same files used for MZmine and XCMS) from the experimental and control groups were analyzed separately using ProteinPilot software version 4.2 (Ab Sciex, Foster City, CA, USA) with the Paragon algorithm. MS^1 and MS^2 data were searched against the *Bos taurus* SwissProt sequence database (6006 reviewed proteins+common protein contaminants, February 2019 release). The parameters input was: sample type, identification; digestion, none; Cys alkylation, none; instrument, TripleTOF 5600; special factors, none; species, *Bos taurus*; ID focus, biological modifications, and amino acid substitutions; search effort, thorough ID. False discovery rate analysis was also performed. All peptides were exported and those with a >90% confidence were linked to the corresponding feature extracted by the XCMS algorithm using their accurate mass and retention time information. For peptide quantification, we employed the normalized feature abundances (MS^1 level) generated by XCMS. A significance threshold of *p<0.05* (Welch's t test) was utilized.

2.8 Proteomics data reprocessing

The SWATH-based proteomics data (identifier PXD013643), hosted in ProteomeXchange consortium via PRIDE (31), was reanalyzed with some modifications. The parameters used to build the spectral library remained the same (15), while the parameter for peptides per protein was set to 100 in the software SWATH® Acquisition MicroApp 2.0 in PeakView® version 1.2 (AB Sciex, Foster City, CA, USA). The obtained protein peak areas were exported to Markerview™ version 1.3 (AB Sciex, Foster City, CA, USA) for further data refinement, including assignment of IDs to files and removal of reversed and common contaminants. Peak areas were exported in a .tsv file, and normalized with NormalyzerDE online version 1.3.4 (32). The NormalyzerDE pipeline comprises 8 different normalization methods (Log2, variance stabilizing normalization, total intensity, median, mean, quantile, CycLoess, and robust linear regression). The results of qualitative (MA plots, scatter plots, box plots, density plots) and quantitative (pooled intragroup coefficient of variation [PCV], median absolute deviation [PMAD], estimate of variance [PEV]) parameters were compared between the normalization methods to select the most appropriate.

2.9 Bioinformatic analysis of proteomics data

Proteins that passed the significance threshold were first converted to their corresponding Entrez Gene (GeneID) using https://www.uniprot.org/uploadlists/ and then transformed to their human equivalents using the ortholog conversion feature in https://biodbnet-abcc.ncifcrf.gov/db/dbOrtho.php. Bioinformatic analysis was done on OmicsNet website platform

7

219   (https://www.omicsnet.ca/) (33, 34). First, a protein-protein interaction (PPI) molecular network

220   (first-order network containing query or seeds molecules and their immediate interacting partners)

221   using STRING PPI database was built (35) and then pathway enrichment analysis was performed

222   using the built-in REACTOME and the Kyoto Encyclopedia of Genes and Genomes (KEGG)

223   databases. To visualize modules (functional units) contained in the molecular network the

224   WalkTrap algorithm (within OmicsNet platform) was employed. Hypergeometric test was used to

225   compute *p-values*.

226

227   **2.10 Integrative analysis of proteomics and metabolomics data**

228   The molecular interactions between the proteins and metabolites differentially abundant between

229   HG + HI and NG were determined in OmicsNet (32, 33). The lists of proteins (EntrezGene ID)

230   and metabolites (HMDB ID) were loaded to build a composite network using protein-protein

231   (STRING database selected) and metabolite-protein (KEGG database selected) interaction types.

232   The primary network relied on the metabolite input. Pathway enrichment analysis was performed

233   using the built-in REACTOME and KEGG databases. Hypergeometric test was used to compute

234   *p-values.*

235

236   **2.11 Statistical analysis**

237   All experiments were performed in triplicate. Based on the accuracy (determination of real fold-

238   changes) of SWATH-based quantification (36), proteins with a fold change ≥ 1.2 or ≤ 1/1.2 and a

239   *p-value* <0.05 (Welch's t-test) were considered as differentially abundant between NG and HG +

240   HI conditions. For the metabolomics data, features with a fold change ≥ 1.3 or ≤ 1/1.3 and a *p-*

241   *value* <0.05 (Welch's t-test) were considered as differentially abundant. We did not apply multiple-

242   test corrections to calculate adjusted p-values, because this process could obscure proteins or

243   metabolites with real changes (true-positives) (37). Instead, the analysis was focused on top-

244   enriched signaling pathways (adjusted *p-value* <0.01) that allowed us to determine a set of

245   interacting proteins and metabolites with relevant biological information and contributes in

246   reducing false positives. For multivariate statistical analysis and heatmap visualization,

247   Metaboanalyst 4.0 (https://www.metaboanalyst.ca) was utilized. Principal component analysis

248   (PCA) was used to assess for sample clustering behavior and inter-group variation. No scaling

249   was used for PCA and heatmap analysis. Software PRISM 6.0 (GraphPad Software, San Diego,

250   CA) was used for the creation of volcano plots and column graphs.

251

252   **2.12 Data availability**

253   The raw datasets supporting the metabolomics results are available in the GNPS/MassIVE public

254   repository (38) under the accession number MSV000084307. The specific parameters of the tools

255   employed for metabolite annotation are available on the following links: for classical molecular

256   networking,

257   https://gnps.ucsd.edu/ProteoSAFe/status.jsp?task=604b3d077e00430a9bc288eebf154b9b;   for

258   FBMN

259   https://gnps.ucsd.edu/ProteoSAFe/status.jsp?task=5e2839037969442e868d9df21309d561;   for

260   NAP,

261   https://proteomics2.ucsd.edu/ProteoSAFe/status.jsp?task=96cda48c0df64d3398a8f9088907afb

262   5; for MS2LDA, http://ms2lda.org/basicviz/summary/1197/ (need to log-in as a registered or guest

263   user);   for   MolNetEnhancer,

264   https://gnps.ucsd.edu/ProteoSAFe/status.jsp?task=de80b9c765e042ffab7767a3101054fd.   The

265   quantitative results generated using the XCMS platform can be accessed after logging into the

266   following link https://xcmsonline.scripps.edu and searching for the job number 1395724. SWATH

267   data is accessible on the ProteomeXchange with dataset identifier PXD013643.

268

269   **3. Results**

270

271   *Untargeted metabolomics*

272   Overall 5571 features or potential metabolites were detected using XCMS and MZmine, wherein

273   957 (~18%) features were commonly identified in both platforms (**Figure 2A**). Based on the

274   relative quantification using XCMS, 140 and 82 features were detected with reduced and

275   increased abundances respectively in the experimental group compared to the control group

276   (**Figure 2B**). The effects of HG and HI in the experimental group are observed by PCA analysis

277   wherein the experimental samples clustered away from the control group (**Figure 2C**). The

278   consistency of the LC-MS equipment is apparent by the clustering of the QC samples (**Figure

279   2C**). Further, the heatmap visualization of the top 100-modulated metabolites exhibited the

280   different distribution patterns among groups (**Figure 2D**). Using the GNPS platform for automatic

281   metabolite annotation, 106 compounds (excluding duplicates and contaminants) were putatively

282   annotated with a level 2 confidence annotation (MS^2 spectral match) (**Table S1**) in agreeance

283   with the MSI classification (28). Some metabolites identified by the GNPS platform could not be

284   quantified because they were not detected by the XCMS algorithm during feature area

285   normalization and quantification. Moreover, GNPS Molecular Networking aligned the MS^2-

286   containing features (n=1,013) based on their structural similarity, creating 118 independent

287   networks or clusters with at least two connected nodes (**Figure 3A**). The use of MolNetEnhancer

9

288   workflow allowed to putatively identify chemical classes (level 3, MSI) for 56 of the 118

289   independent networks. The top-10 most abundant annotated chemical classes and associated

290   metabolites are shown in **Figure 3A.** Three-clusters from the network were further analyzed

291   because they contained annotated metabolites by spectral matching, which facilitates the

292   annotation of other cluster's nodes. Cluster 1 revealed two metabolites linked to the

293   organonitrogen compounds class with reduced abundance in the experimental group (**Figure 3B**).

294   Library spectral match (level 2, MSI) suggest PC(16:0/18:1(9Z)) and PC(18:0/18:2(9Z,12Z)) as

295   putative candidates, which was supported by MS2LDA phosphocholine-substructure recognition

296   (**Figure 3C**). In cluster 2, glutathione-based metabolites (MSI level 3) were detected through

297   fragments *m/z* 308.0925, 233.0575, 179.0475, and 162.0225 retrieved by the M2M_453

298   substructure and associated with glutathione structure using mzCloud *in silico* predictions (**Figure**

299   **4A**). The precursor ion at *m/z* 713.1472 and glutathione (annotated at level 2, MSI) were detected

300   with increased abundance in the experimental group. MS2LDA visualization, at the M2M level,

301   correlated with the GNPS molecular networking clustering (**Figure 4B**). In cluster 3, various

302   phenylalanine-based metabolites were putatively annotated aided by MS2LDA substructure

303   recognition (**Figure 4C and 4D**). Within this cluster, glutamyl-phenylalanine (annotated at level 2,

304   MSI) and the precursor ions at *m/z* 297.1802 and 487.1548 presented with increased abundance

305   in the experimental vs. control group. On the other hand, various aminoacids were annotated

306   (level 2, MSI) by GNPS spectral matching and manual inspection of data (**Table S2**). Threonine,

307   valine, proline, leucine, serine, glutamic acid, methionine, and tyrosine presented increased

308   abundance (fold change range 1.3-1.7, $p<0.05$) in the experimental vs. control group. Particularly,

309   metabolites linked to the catabolism of tryptophan via the serotonin and kynurenine pathway (39)

310   were annotated (level 2, MSI), including melatonin, acetyl serotonin, and kynurenine (**Table S1**).

311   However, only kynurenine was significantly elevated in the experimental group. The full list of

312   annotated metabolites, differential abundances and another relevant feature information is shown

313   in **Table S2**.

314

315   *Peptidomics*

316   Experimental and control datasets were analyzed separately to identify the peptides and their

317   biological modifications. The complete list of peptides identified by ProteinPilot between the

318   experimental and control groups are described in **Table S3.** Proline oxidation was the most

319   frequent biological modification detected in the experimental group datasets. We identified 8 and

320   12 peptides with a confidence of >90% in the control and experimental group, respectively.

321   Differential abundance of 2 proline-rich peptides was observed in the experimental group

322   compared to the control group. An additional tripeptide was manually annotated with a LPP

323   sequence (**Table S4**).

324

325   *Proteomics*

326   The re-analysis of the SWATH data (PXD013643 dataset) facilitated the identification of 952

327   quantifiable proteins (717 proteins with at least 2 unique peptides, 1% false discovery rate) and

328   no missing values among technical and biological replicates (**Table S5**). Sample datasets were

329   normalized using 8 different methods to select the most appropriate based on quantitative and

330   qualitative parameters on our dataset. Quantile normalization produced a better qualitative and

331   quantitative profile and was selected to further process our data (**Figure S1**). PCA analysis of

332   normalized data denoted a clear separation of the groups suggesting overall differences in their

333   proteomes (**Figure 5A**). Differential abundance analysis revealed 32 and 33 proteins with

334   increased and decreased abundance in the experimental group (**Figure 5B**). Further, the

335   heatmap visualization of the top 50-modulated proteins exhibited the different distribution patterns

336   among the experimental and control groups (**Figure 5C**). To obtain a molecular insight we

337   performed a functional enrichment analysis using a network-based approach. First, we created a

338   composite network comprising PPI between the modulated proteins by simulated diabetes (seed

339   proteins) and their immediate interacting partners (highest confidence >0.9) retrieved from

340   STRING Database (incorporated in OmicsNet platform). The principal network using the up-

341   modulated proteins consisted of 461 proteins, 709 edges and 18 seed proteins (nodes with blue

342   shadow) and is illustrated in **Figure 5D**. Eight modules or clusters were generated, that may

343   represent relevant complexes or functional units (40). The 5 most significant (adjusted p-value

344   <0.05) REACTOME and KEGG pathways on the global network are shown in **Table 1**. Two

345   modules contained multiple seed proteins and were linked to DNA/RNA and protein metabolism

346   pathways using the WalkTrap algorithm (**Figure 5D**). On the other hand, the principal network

347   using the down-modulated proteins consisted of 488 proteins, 513 edges and 18 seed proteins

348   identified eleven modules wherein one module (with 2 seed proteins) indicated associations with

349   mitochondrial function pathways (**Figure 5E**).

350

351   *Integration of Metabolomics and Proteomics*

352   The signaling pathways perturbed by simulated diabetes were identified by a composite network

353   of interacting metabolites and proteins using OmicsNet built-in databases. **Figure 6** illustrates the

354   composite bi-layered metabolite-PPI network using the up-modulated molecules (under simulated

355   diabetes) comprised of 9 metabolites (seed metabolites), 177 edges, and 166 proteins (5 seed

11

356   proteins). The 10 top-most enriched signaling pathways identified in the composite network are

357   shown in **Table 2**. The two principal modules highlighted by the WalkTrap algorithm were linked

358   to glutathione and amino acid metabolism. We noted a smaller interaction between Acyl-protein

359   thioesterase 1 (LYPLA1) and a phosphatidylcholine metabolite when simultaneously analyzing

360   up- and down-modulated proteins and metabolites. No significant composite network was

361   identified using the down-modulated proteins and metabolites.

362

363   *Cellular morphology*

364   To better understand the effects that simulated diabetes exerts on endothelial cells the changes

365   on cellular structure endpoints were evaluated. The endothelial nuclei morphology in the BCAEC

366   control and experimental groups were evaluated using fluorescent-staining and image analysis.

367   We also evaluated the presence of vWF (marker of endothelial cells) in BCAEC and HCAEC, to

368   reveal the cellular boundary and to demonstrate their endothelial phenotype (41). We noted an

369   increase in the percentage of binucleated BCAEC in the experimental group compared to the

370   control group (top panel **Figure 7A and 7B**). A similar result with larger nuclei, was observed

371   when using HCAEC as a human *in vitro* model (bottom panel **Figure 7A and 7B**). Finally, as

372   expected, we observed a typical intracellular localization of vWF and a 100% positivity in

373   endothelial cells.

374

375   **4. Discussion**

376   This study investigated the molecular perturbations occurring in coronary endothelium cells

377   subjected to prolonged simulated diabetes that facilitated the identification of signaling pathways

378   and specific molecules that could be associated with the development of cardiovascular disease.

379   To achieve this, we employed a MS-based multi-omics approach coupled to fluorescence

380   microscopy to detect structural changes. Endothelial cells cover the inner surface of blood vessels

381   and are distributed across the body. Their functions include: acting as a mechanical barrier

382   between the circulating blood and adjacent tissues as well as modulating multiple functions in

383   distinct organs (42). These regulatory functions vary according to localization and vascular bed-

384   origin (43). HG blood levels are detrimental to endothelial cells function in T2DM leading to

385   coronary endothelial dysfunction and development of CVD (44, 45). The molecular effects of HG

386   on endothelial cells have been previously characterized (4, 6, 7, 10, 11); nevertheless, the

387   endothelial cell types used in these studies are not intrinsically involved in CVD. The present study

388   used an *in vitro* model involving endothelial cells that modulate the heart function, CAEC (46).

389   Our model not only used HG (20 mmol/L) to simulate diabetes (4, 6, 7, 10, 11) but first induced

390   insulin resistance to mimic the pathophysiological conditions that occur in T2DM wherein

391   hyperinsulinemia precedes hyperglycemia (18). Diabetes was simulated for up to 12 days to

392   mimic chronic HG exposure and to prevent measuring cell proliferation known to occur in early

393   HG (10, 16). Despite a lack of apparent increase in cell proliferation in the experimental group

394   compared to control group after twelve days, an increase in overall protein abundance was

395   detected by Bradford assay (data not shown) and inferred from total ion chromatogram (TIC) of

396   MS (**Figure S1A**). We suggest that protein synthesis is increased as a consequence of the higher

397   presence of bi-nucleated CAEC (with increased DNA/RNA metabolism) under HG + HI compared

398   to that in the control cohort (**Figure 7A and 7B**). Previous studies have shown reduced endothelial

399   cell proliferation (mostly in HUVEC) after long-term (7-14 days) HG exposure (4, 11, 47-53),

400   accompanied by an increase in protein synthesis (53). This MS-based methodological pipeline

401   that included appropriate controls during data acquisition (QC) and processing (e.g.,

402   normalization, filtering, annotation, dereplication, etc.), allowed the identification of global

403   changes in the metabolome of CAEC under HG + HI. Specifically, increased abundance of valine,

404   leucine, tyrosine, serine, leucine, proline, methionine, and glutamic acid in cells under HG

405   conditions was observed; and this is consistent with reports on human aortic endothelial cells

406   (54). Notably, several clinical studies have established a direct relationship between

407   prevalence/incidence of T2DM and increased levels of valine, leucine and tyrosine in serum and

408   plasma (55-59). Our results support the role of CAEC in contributing to the elevated pool of amino

409   acids seen in circulation under a HG environment. We speculate that increased levels of these

410   amino acids could result from either increased production or reduced degradation as suggested

411   in endothelial cells (immortalized cell line, EA.hy 926) that transition from a glycolytic metabolism

412   towards lipid and amino acid oxidation when challenged by HG (60). Furthermore, evidence of

413   increased tryptophan catabolism was identified through the kynurenine pathway. In this regard, a

414   non-significant decrease of ~ 40% in the abundance of tryptophan was detected. However, a

415   significant increase of ~ 450% in kynurenine (tryptophan's main metabolite) (61) between the HG

416   + HI group and NG group was also observed, which is a key finding as elevated plasma levels of

417   kynurenine are known to increase CVD risk (62, 63). This novel finding contributes to expanding

418   the understanding of amino acid metabolism in endothelial cells under simulated diabetes. Acetyl

419   serotonin and melatonin which are components of the serotonin pathway that degrades

420   tryptophan (64) were also detected with only minor abundancy increases (20-30%) in the HG +

421   HI group compared to control. Differences in glutathione (cysteine-glutamic acid-glycine,

422   tripeptide) metabolism in CAEC were also found, suggesting an increased response to oxidative

423   stress (65). In line with this observation, previous research reported a glutathione-dependent

13

424　reaction to ambient HG in artery-derived endothelial cells (66, 67) but the same could not be

425　observed in vein-derived endothelial cells (68, 69). This emphasizes the different responses to

426　HG among endothelial phenotypes. Here, novel evidence is provided of the up-regulation of

427　glutathione-based metabolites. The composite protein network suggested an increase in

428　glutathione metabolism supported by elevated levels of oxidized glutathione and, one of its

429　synthetic precursors, glutamic acid. At the protein level, peroxiredoxin (PRDX2 and PRDX6) and

430　thioredoxin (TXN2, mitochondrial) showed increased abundances in the experimental group,

431　which are part of the cells natural enzymatic defense against oxidative stress (70). The

432　substructure analysis of metabolomics data facilitated identifying glutamic acid- and

433　phenylalanine-based metabolites, presumably di- or tri-peptides, including the annotated

434　metabolite glutamyl-phenylalanine. Furthermore, the CAEC peptidome analysis suggested an

435　increase in proline-containing peptides. This type of peptide is of particular interest because of

436　their resistance to non-specific proteolytic degradation, body distribution and remarkable

437　biological effects (71-74). Yet, the precise function of such phenylalanine-, glutamine-, and

438　proline-based peptides remains to be characterized in CAEC. We can only speculate that they

439　are the result of a compensatory mechanism to reduce glucose cellular damage. Also, increased

440　protein abundance of core and regulatory subunits from the proteasome complex (PSMA4 and

441　PSMD3) was found in cells under simulated diabetes. This suggests an increased protein

442　degradation and subsequent peptide formation in response to HG. Metabolomic profiling also

443　revealed changes in the lipidome of CAEC challenged with HG + HI, wherein a reduction in

444　phosphatidylcholine (PC) lipids and subsequent increase in phosphocholine were noted.

445　Changes in the phospholipidomic profile of bovine aortic endothelial cells treated with HG for 24

446　h has also been reported in a lipidome study (75). Here, proteomics and metabolomics data were

447　manually integrated and this allowed to determine critical roles for PAFAH1B2 and LYPLA1 in

448　mediating the degradation of PC lipids (**Figure 8**). PAFAH1B2 was found to be up-regulated in

449　this study and it is known to be associated with inflammation and higher levels of lysoPC (76). As

450　a result, PAFAH1B2 could increase the pool of lysoPC lipids, further exacerbating inflammation

451　in the cardiovascular system (77). On the other hand, LYPLA1 has a lysophospholipase activity

452　that can hydrolyze a range of lysophospholipids, including LysoPC, thereby generating a fatty

453　acid and glycerophosphocholine as products (78). Increased levels of phosphocholine (~ 460%)

454　were detected in HG treated cells compared to control, that could be associated with the

455　degradation of LysoPC lipids. It should be noted that the use of pathways databases such as

456　KEGG and REACTOME possess some limitations when dealing with lipid metabolites because

457　its chemical diversity is not well annotated/defined within the databases. For example, KEGG

14

458 provides a chemical class identifier instead of individual identity to lipids, constricting their

459 biological importance (79). Thus, based on our manual inspection of the metabolomics-

460 proteomics data and in line with the evidence, we suggest that simulated diabetes evokes

461 inflammation on BCAEC and that PAFAH1B2 and LYPLA1 play a role in modulating such

462 process.

463 Previously, we reported the multinucleation of CAEC cultured under simulated diabetes (15). This

464 type of cell possesses ≥2 nuclei. Here, we replicated our previous findings of increased

465 binucleation in BCAEC. The same outcome was obtained when using HCAEC as a human *in vitro*

466 model (**Figure 7A and 7B**), validating the binucleation process in other CAEC. After refinement

467 of LC-MS^2 data and bioinformatics re-processing of published SWATH-based datasets of BCAEC

468 under simulated diabetes (15), molecular signatures and pathways that could be linked to the

469 binucleation process were found (**Figure 8**). For instance, we noted an increased abundance of

470 proteins, under simulated diabetes, with reported nuclei localization and linked to DNA

471 metabolism, including ribosomal proteins RPS7, RPS13, and RPL9 (80). Further, we observed

472 an increased abundance of proteasome proteins, PSMA4 and PSMD3, which are linked to protein

473 metabolism (81). Hence, we infer that the CAEC binucleation occurs as a compensatory

474 mechanism to increase the cell capacity to metabolize the excess of ambient glucose by

475 increasing the cell metabolic machinery (transcription/translation processes). Although an

476 increase in cell proliferation could boost a coordinated increase of ribosomal and proteasome

477 proteins, we do not believe this is the case here, as mentioned before. After 4-5 days of simulated

478 diabetes, cells occupied 100% of the well's plate surface, thereby impeding to harbor more cells

479 because endothelial cells grow as a monolayer. This is consistent with findings stating that when

480 endothelial cells become highly confluent, they stop growing due to cell-cell contact, even in the

481 presence of growth factors (82). In support of this, up-stream (CTGF and CD62) (83, 84) (**Table**

482 **S5**) and down-stream proteins (FABP4) (85) (**Table S5**) involved in angiogenesis and proliferation

483 were down-regulated by simulated diabetes. Importantly, there is evidence (not in endothelial

484 cells) of cellular processes contributing to the stimulation of cellular binucleation without increases

485 in cell proliferation, including cellular enhancement of antimicrobial defenses (86), senescence

486 (87), and malignancy (88). Various mechanisms have been linked to the binucleation process,

487 such as cytokinesis failure, cellular fusion, mitotic slippage, and endoreduplication (89). The

488 elucidation of the exact molecular mechanisms leading to the binucleation process of CAEC is

489 beyond the scope of our study.

490 In conclusion, this study applied an integrated multi-omics and bioinformatics/chemoinformatics

491 approach to characterize the molecular perturbations that simulated diabetes exerts on CAEC.

492   We confirmed several independent studies that reported alterations at protein and metabolite
493   levels in endothelial cells of different sources than coronary vessels. Metabolomics, identified
494   alterations in amino acid, peptide, and phospholipid metabolism. Notably, the chemoinformatic
495   analysis identified unreported alterations of phenylalanine-, glutathione-, and proline-based
496   peptides on coronary endothelium under simulated diabetes. Proteomics provided evidence of
497   reduced mitochondrial mass and angiogenesis. The integration of proteomics and metabolomics
498   identified increased glutamic acid metabolism and suggested that the antioxidant enzymes are
499   involved in protecting the cells from oxidative stress. Fluorescence microscopy reported the
500   appearance of non-proliferative binucleated CAEC cells as a mean to metabolize the excess of
501   ambient glucose. Overall, our study improved the understanding of the molecular disturbances
502   caused by simulated diabetes that could mediate CAEC dysfunction and may be relevant in the
503   context of CVD in subjects with T2DM.

504
505

16

506 **5. Acknowledgements**

507 This work was derived in part from the Thesis Project of H.C.D.H. at the Posgrado en

508 Ciencias de la Vida, CICESE. We thank Alan G. Hernández-Melgar for his invaluable

509 technical assistance with the NormalyzerDE software.

510

511

512

513

514

515

520

521

522 **7. Conflict of interest**

523   Dr. Villarreal is a co-founder and stockholder of Cardero Therapeutics, Inc.

524

525

526   **8. Author contributions**

527   A.M.U. contributed to the study conception and design, data acquisition, formal analysis,

528   methodology, project administration, and funding acquisition. H.C.D.H., L.D.M, and R.A.C.C.

529   contributed to the data acquisition, formal analysis and interpretation of some experiments.

530   C.A.D., and F.V. contributed to funding acquisition and resources. O.M.P contributed to data

531   interpretation and critical revision of manuscript. All authors contributed to the drafting, revising,

532   and approval of the final version of the manuscript.

533

References

1.   Halcox, J. P.; Schenke, W. H.; Zalos, G.; Mincemoyer, R.; Prasad, A.; Waclawiw, M. A.; Nour, K. R.; Quyyumi, A. A., Prognostic value of coronary vascular endothelial dysfunction. *Circulation* **2002,** 106, (6), 653-8.

2.   Lind, M.; Wedel, H.; Rosengren, A., Excess Mortality among Persons with Type 2 Diabetes. *N Engl J Med* **2016,** 374, (8), 788-9.

3.   Gutierrez, E.; Flammer, A. J.; Lerman, L. O.; Elizaga, J.; Lerman, A.; Fernandez-Aviles, F., Endothelial dysfunction over the course of coronary artery disease. *Eur Heart J* **2013,** 34, (41), 3175-81.

4.   Lorenzi, M.; Cagliero, E.; Toledo, S., Glucose toxicity for human endothelial cells in culture. Delayed replication, disturbed cell cycle, and accelerated death. *Diabetes* **1985,** 34, (7), 621-7.

5.   Kageyama, S.; Yokoo, H.; Tomita, K.; Kageyama-Yahara, N.; Uchimido, R.; Matsuda, N.; Yamamoto, S.; Hattori, Y., High glucose-induced apoptosis in human coronary artery endothelial cells involves up-regulation of death receptors. *Cardiovasc Diabetol* **2011,** 10, 73.

6.   Dubois, S.; Madec, A. M.; Mesnier, A.; Armanet, M.; Chikh, K.; Berney, T.; Thivolet, C., Glucose inhibits angiogenesis of isolated human pancreatic islets. *J Mol Endocrinol* **2010,** 45, (2), 99-105.

7.   Lorenzi, M.; Montisano, D. F.; Toledo, S.; Barrieux, A., High glucose induces DNA damage in cultured human endothelial cells. *J Clin Invest* **1986,** 77, (1), 322-5.

8.   Patel, H.; Chen, J.; Das, K. C.; Kavdia, M., Hyperglycemia induces differential change in oxidative stress at gene expression and functional levels in HUVEC and HMVEC. *Cardiovasc Diabetol* **2013,** 12, 142.

9.   Pala, L.; Pezzatini, A.; Dicembrini, I.; Ciani, S.; Gelmini, S.; Vannelli, B. G.; Cresci, B.; Mannucci, E.; Rotella, C. M., Different modulation of dipeptidyl peptidase-4 activity between microvascular and macrovascular human endothelial cells. *Acta Diabetol* **2012,** 49 Suppl 1, S59-63.

10.   Esposito, C.; Fasoli, G.; Plati, A. R.; Bellotti, N.; Conte, M. M.; Cornacchia, F.; Foschi, A.; Mazzullo, T.; Semeraro, L.; Dal Canton, A., Long-term exposure to high glucose up-regulates VCAM-induced endothelial cell adhesiveness to PBMC. *Kidney Int* **2001,** 59, (5), 1842-9.

11.   Baumgartner-Parzer, S. M.; Wagner, L.; Pettermann, M.; Grillari, J.; Gessl, A.; Waldhausl, W., High-glucose--triggered apoptosis in cultured endothelial cells. *Diabetes* **1995,** 44, (11), 1323-7.

12.   Ramirez-Sanchez, I.; Rodriguez, A.; Moreno-Ulloa, A.; Ceballos, G.; Villarreal, F., (-)-Epicatechin-induced recovery of mitochondria from simulated diabetes: Potential role of endothelial nitric oxide synthase. *Diab Vasc Dis Res* **2016,** 13, (3), 201-10.

13.   Liu, T.; Gong, J.; Chen, Y.; Jiang, S., Periodic vs constant high glucose in inducing pro-inflammatory cytokine expression in human coronary artery endothelial cells. *Inflamm Res* **2013,** 62, (7), 697-701.

14.   Liu, T. S.; Pei, Y. H.; Peng, Y. P.; Chen, J.; Jiang, S. S.; Gong, J. B., Oscillating high glucose enhances oxidative stress and apoptosis in human coronary artery endothelial cells. *J Endocrinol Invest* **2014,** 37, (7), 645-51.

15.   Hilda Carolina Delgado De la Herrán, L. D.-M., Carolina Álvarez-Delgado, Francisco Villarreal, Aldo Moreno-Ulloa, Formation of multinucleated variant endothelial cells with altered mitochondrial function in cultured coronary endothelium under simulated diabetes. *bioRxiv* **2019**.

581   16.   Li, X. X.; Liu, Y. M.; Li, Y. J.; Xie, N.; Yan, Y. F.; Chi, Y. L.; Zhou, L.; Xie, S. Y.; Wang, P.
582   Y., High glucose concentration induces endothelial cell proliferation by regulating cyclin-D2-
583   related miR-98. *J Cell Mol Med* **2016,** 20, (6), 1159-69.
584   17.   Madonna, R.; De Caterina, R., Prolonged exposure to high insulin impairs the
585   endothelial PI3-kinase/Akt/nitric oxide signalling. *Thromb Haemost* **2009,** 101, (2), 345-50.
586   18.   Zaccardi, F.; Webb, D. R.; Yates, T.; Davies, M. J., Pathophysiology of type 1 and type 2
587   diabetes mellitus: a 90-year perspective. *Postgrad Med J* **2016,** 92, (1084), 63-9.
588   19.   Moreno-Ulloa, A.; Miranda-Cervantes, A.; Licea-Navarro, A.; Mansour, C.; Beltran-
589   Partida, E.; Donis-Maturano, L.; Delgado De la Herran, H. C.; Villarreal, F.; Alvarez-Delgado, C.,
590   (-)-Epicatechin stimulates mitochondrial biogenesis and cell growth in C2C12 myotubes via the
591   G-protein coupled estrogen receptor. *Eur J Pharmacol* **2018,** 822, 95-107.
592   20.   Kirkwood, J. S.; Maier, C.; Stevens, J. F., Simultaneous, untargeted metabolic profiling
593   of polar and nonpolar metabolites by LC-Q-TOF mass spectrometry. *Curr Protoc Toxicol* **2013,**
594   Chapter 4, Unit4 39.
595   21.   Moreno-Ulloa, A.; Sicairos Diaz, V.; Tejeda-Mora, J. A.; Macias Contreras, M. I.; Castillo,
596   F. D.; Guerrero, A.; Gonzalez Sanchez, R.; Mendoza-Porras, O.; Vazquez Duhalt, R.; Licea-
597   Navarro, A., Chemical Profiling Provides Insights into the Metabolic Machinery of Hydrocarbon-
598   Degrading Deep-Sea Microbes. *mSystems* **2020,** 5, (6).
599   22.   Gowda, H.; Ivanisevic, J.; Johnson, C. H.; Kurczy, M. E.; Benton, H. P.; Rinehart, D.;
600   Nguyen, T.; Ray, J.; Kuehl, J.; Arevalo, B.; Westenskow, P. D.; Wang, J.; Arkin, A. P.;
601   Deutschbauer, A. M.; Patti, G. J.; Siuzdak, G., Interactive XCMS Online: simplifying advanced
602   metabolomic data processing and subsequent statistical analyses. *Anal Chem* **2014,** 86, (14),
603   6931-9.
604   23.   Pluskal, T.; Castillo, S.; Villar-Briones, A.; Oresic, M., MZmine 2: modular framework for
605   processing, visualizing, and analyzing mass spectrometry-based molecular profile data. *BMC*
606   *Bioinformatics* **2010,** 11, 395.
607   24.   Aron, A. T.; Gentry, E. C.; McPhail, K. L.; Nothias, L. F.; Nothias-Esposito, M.;
608   Bouslimani, A.; Petras, D.; Gauglitz, J. M.; Sikora, N.; Vargas, F.; van der Hooft, J. J. J.; Ernst,
609   M.; Kang, K. B.; Aceves, C. M.; Caraballo-Rodriguez, A. M.; Koester, I.; Weldon, K. C.;
610   Bertrand, S.; Roullier, C.; Sun, K.; Tehan, R. M.; Boya, P. C.; Christian, M. H.; Gutierrez, M.;
611   Ulloa, A. M.; Tejeda Mora, J. A.; Mojica-Flores, R.; Lakey-Beitia, J.; Vasquez-Chaves, V.;
612   Zhang, Y.; Calderon, A. I.; Tayler, N.; Keyzers, R. A.; Tugizimana, F.; Ndlovu, N.; Aksenov, A.
613   A.; Jarmusch, A. K.; Schmid, R.; Truman, A. W.; Bandeira, N.; Wang, M.; Dorrestein, P. C.,
614   Reproducible molecular networking of untargeted mass spectrometry data using GNPS. *Nat*
615   *Protoc* **2020**.
616   25.   da Silva, R. R.; Wang, M.; Nothias, L. F.; van der Hooft, J. J. J.; Caraballo-Rodriguez, A.
617   M.; Fox, E.; Balunas, M. J.; Klassen, J. L.; Lopes, N. P.; Dorrestein, P. C., Propagating
618   annotations of molecular networks using in silico fragmentation. *PLoS Comput Biol* **2018,** 14,
619   (4), e1006089.
620   26.   van der Hooft, J. J.; Wandy, J.; Barrett, M. P.; Burgess, K. E.; Rogers, S., Topic
621   modeling for untargeted substructure exploration in metabolomics. *Proc Natl Acad Sci U S A*
622   **2016,** 113, (48), 13738-13743.
623   27.   Djoumbou Feunang, Y.; Eisner, R.; Knox, C.; Chepelev, L.; Hastings, J.; Owen, G.;
624   Fahy, E.; Steinbeck, C.; Subramanian, S.; Bolton, E.; Greiner, R.; Wishart, D. S., ClassyFire:
625   automated chemical classification with a comprehensive, computable taxonomy. *J Cheminform*
626   **2016,** 8, 61.
627   28.   Schymanski, E. L.; Jeon, J.; Gulde, R.; Fenner, K.; Ruff, M.; Singer, H. P.; Hollender, J.,
628   Identifying small molecules via high resolution mass spectrometry: communicating confidence.
629   *Environ Sci Technol* **2014,** 48, (4), 2097-8.

630 29.   Ernst, M.; Kang, K. B.; Caraballo-Rodriguez, A. M.; Nothias, L. F.; Wandy, J.; Chen, C.;
631 Wang, M.; Rogers, S.; Medema, M. H.; Dorrestein, P. C.; van der Hooft, J. J. J.,
632 MolNetEnhancer: Enhanced Molecular Networks by Integrating Metabolome Mining and
633 Annotation Tools. *Metabolites* **2019,** 9, (7).
634 30.   Shannon, P.; Markiel, A.; Ozier, O.; Baliga, N. S.; Wang, J. T.; Ramage, D.; Amin, N.;
635 Schwikowski, B.; Ideker, T., Cytoscape: a software environment for integrated models of
636 biomolecular interaction networks. *Genome Res* **2003,** 13, (11), 2498-504.
637 31.   Perez-Riverol, Y.; Csordas, A.; Bai, J.; Bernal-Llinares, M.; Hewapathirana, S.; Kundu,
638 D. J.; Inuganti, A.; Griss, J.; Mayer, G.; Eisenacher, M.; Perez, E.; Uszkoreit, J.; Pfeuffer, J.;
639 Sachsenberg, T.; Yilmaz, S.; Tiwary, S.; Cox, J.; Audain, E.; Walzer, M.; Jarnuczak, A. F.;
640 Ternent, T.; Brazma, A.; Vizcaino, J. A., The PRIDE database and related tools and resources
641 in 2019: improving support for quantification data. *Nucleic Acids Res* **2019,** 47, (D1), D442-
642 D450.
643 32.   Willforss, J.; Chawade, A.; Levander, F., NormalyzerDE: Online Tool for Improved
644 Normalization of Omics Expression Data and High-Sensitivity Differential Expression Analysis. *J
645 Proteome Res* **2019,** 18, (2), 732-740.
646 33.   Zhou, G.; Xia, J., Using OmicsNet for Network Integration and 3D Visualization. *Curr
647 Protoc Bioinformatics* **2019,** 65, (1), e69.
648 34.   Zhou, G.; Xia, J., OmicsNet: a web-based tool for creation and visual analysis of
649 biological networks in 3D space. *Nucleic Acids Res* **2018,** 46, (W1), W514-W522.
650 35.   Szklarczyk, D.; Franceschini, A.; Wyder, S.; Forslund, K.; Heller, D.; Huerta-Cepas, J.;
651 Simonovic, M.; Roth, A.; Santos, A.; Tsafou, K. P.; Kuhn, M.; Bork, P.; Jensen, L. J.; von
652 Mering, C., STRING v10: protein-protein interaction networks, integrated over the tree of life.
653 *Nucleic Acids Res* **2015,** 43, (Database issue), D447-52.
654 36.   Muntel, J.; Kirkpatrick, J.; Bruderer, R.; Huang, T.; Vitek, O.; Ori, A.; Reiter, L.,
655 Comparison of Protein Quantification in a Complex Background by DIA and TMT Workflows
656 with Fixed Instrument Time. *J Proteome Res* **2019,** 18, (3), 1340-1351.
657 37.   Pascovici, D.; Handler, D. C.; Wu, J. X.; Haynes, P. A., Multiple testing corrections in
658 quantitative proteomics: A useful but blunt tool. *Proteomics* **2016,** 16, (18), 2448-53.
659 38.   Wang, M.; Carver, J. J.; Phelan, V. V.; Sanchez, L. M.; Garg, N.; Peng, Y.; Nguyen, D.
660 D.; Watrous, J.; Kapono, C. A.; Luzzatto-Knaan, T.; Porto, C.; Bouslimani, A.; Melnik, A. V.;
661 Meehan, M. J.; Liu, W. T.; Crusemann, M.; Boudreau, P. D.; Esquenazi, E.; Sandoval-Calderon,
662 M.; Kersten, R. D.; Pace, L. A.; Quinn, R. A.; Duncan, K. R.; Hsu, C. C.; Floros, D. J.; Gavilan,
663 R. G.; Kleigrewe, K.; Northen, T.; Dutton, R. J.; Parrot, D.; Carlson, E. E.; Aigle, B.; Michelsen,
664 C. F.; Jelsbak, L.; Sohlenkamp, C.; Pevzner, P.; Edlund, A.; McLean, J.; Piel, J.; Murphy, B. T.;
665 Gerwick, L.; Liaw, C. C.; Yang, Y. L.; Humpf, H. U.; Maansson, M.; Keyzers, R. A.; Sims, A. C.;
666 Johnson, A. R.; Sidebottom, A. M.; Sedio, B. E.; Klitgaard, A.; Larson, C. B.; P, C. A. B.; Torres-
667 Mendoza, D.; Gonzalez, D. J.; Silva, D. B.; Marques, L. M.; Demarque, D. P.; Pociute, E.;
668 O'Neill, E. C.; Briand, E.; Helfrich, E. J. N.; Granatosky, E. A.; Glukhov, E.; Ryffel, F.; Houson,
669 H.; Mohimani, H.; Kharbush, J. J.; Zeng, Y.; Vorholt, J. A.; Kurita, K. L.; Charusanti, P.; McPhail,
670 K. L.; Nielsen, K. F.; Vuong, L.; Elfeki, M.; Traxler, M. F.; Engene, N.; Koyama, N.; Vining, O. B.;
671 Baric, R.; Silva, R. R.; Mascuch, S. J.; Tomasi, S.; Jenkins, S.; Macherla, V.; Hoffman, T.;
672 Agarwal, V.; Williams, P. G.; Dai, J.; Neupane, R.; Gurr, J.; Rodriguez, A. M. C.; Lamsa, A.;
673 Zhang, C.; Dorrestein, K.; Duggan, B. M.; Almaliti, J.; Allard, P. M.; Phapale, P.; Nothias, L. F.;
674 Alexandrov, T.; Litaudon, M.; Wolfender, J. L.; Kyle, J. E.; Metz, T. O.; Peryea, T.; Nguyen, D.
675 T.; VanLeer, D.; Shinn, P.; Jadhav, A.; Muller, R.; Waters, K. M.; Shi, W.; Liu, X.; Zhang, L.;
676 Knight, R.; Jensen, P. R.; Palsson, B. O.; Pogliano, K.; Linington, R. G.; Gutierrez, M.; Lopes, N.
677 P.; Gerwick, W. H.; Moore, B. S.; Dorrestein, P. C.; Bandeira, N., Sharing and community

678   curation of mass spectrometry data with Global Natural Products Social Molecular Networking.
679   *Nat Biotechnol* **2016,** 34, (8), 828-837.
680   39.   Bender, D. A., Biochemistry of tryptophan in health and disease. *Mol Aspects Med* **1983,**
681   6, (2), 101-97.
682   40.   Poyatos, J. F.; Hurst, L. D., How biologically relevant are interaction-based modules in
683   protein networks? *Genome Biol* **2004,** 5, (11), R93.
684   41.   Muller, A. M.; Hermanns, M. I.; Skrzynski, C.; Nesslinger, M.; Muller, K. M.; Kirkpatrick,
685   C. J., Expression of the endothelial markers PECAM-1, vWf, and CD34 in vivo and in vitro. *Exp*
686   *Mol Pathol* **2002,** 72, (3), 221-9.
687   42.   Aird, W. C., Phenotypic heterogeneity of the endothelium: II. Representative vascular
688   beds. *Circ Res* **2007,** 100, (2), 174-90.
689   43.   Aird, W. C., Endothelial cell heterogeneity. *Cold Spring Harb Perspect Med* **2012,** 2, (1),
690   a006429.
691   44.   Widlansky, M. E.; Gokce, N.; Keaney, J. F., Jr.; Vita, J. A., The clinical implications of
692   endothelial dysfunction. *J Am Coll Cardiol* **2003,** 42, (7), 1149-60.
693   45.   Ganz, P.; Vita, J. A., Testing endothelial vasomotor function: nitric oxide, a multipotent
694   molecule. *Circulation* **2003,** 108, (17), 2049-53.
695   46.   Paulus, W. J.; Vantrimpont, P. J.; Shah, A. M., Paracrine coronary endothelial control of
696   left ventricular function in humans. *Circulation* **1995,** 92, (8), 2119-26.
697   47.   Abe, M.; Ono, J.; Sato, Y.; Okeda, T.; Takaki, R., Effects of glucose and insulin on
698   cultured human microvascular endothelial cells. *Diabetes Res Clin Pract* **1990,** 9, (3), 287-95.
699   48.   Du, X. L.; Sui, G. Z.; Stockklauser-Farber, K.; Weiss, J.; Zink, S.; Schwippert, B.; Wu, Q.
700   X.; Tschope, D.; Rosen, P., Introduction of apoptosis by high proinsulin and glucose in cultured
701   human umbilical vein endothelial cells is mediated by reactive oxygen species. *Diabetologia*
702   **1998,** 41, (3), 249-56.
703   49.   Graier, W. F.; Grubenthal, I.; Dittrich, P.; Wascher, T. C.; Kostner, G. M., Intracellular
704   mechanism of high D-glucose-induced modulation of vascular cell proliferation. *Eur J Pharmacol*
705   **1995,** 294, (1), 221-9.
706   50.   Kamal, K.; Du, W.; Mills, I.; Sumpio, B. E., Antiproliferative effect of elevated glucose in
707   human microvascular endothelial cells. *J Cell Biochem* **1998,** 71, (4), 491-501.
708   51.   Lorenzi, M.; Nordberg, J. A.; Toledo, S., High glucose prolongs cell-cycle traversal of
709   cultured human endothelial cells. *Diabetes* **1987,** 36, (11), 1261-7.
710   52.   Quagliaro, L.; Piconi, L.; Assaloni, R.; Martinelli, L.; Motz, E.; Ceriello, A., Intermittent
711   high glucose enhances apoptosis related to oxidative stress in human umbilical vein endothelial
712   cells: the role of protein kinase C and NAD(P)H-oxidase activation. *Diabetes* **2003,** 52, (11),
713   2795-804.
714   53.   McGinn, S.; Poronnik, P.; King, M.; Gallery, E. D.; Pollock, C. A., High glucose and
715   endothelial cell growth: novel effects independent of autocrine TGF-beta 1 and hyperosmolarity.
716   *Am J Physiol Cell Physiol* **2003,** 284, (6), C1374-86.
717   54.   Yuan, W.; Zhang, J.; Li, S.; Edwards, J. L., Amine metabolomics of hyperglycemic
718   endothelial cells using capillary LC-MS with isobaric tagging. *J Proteome Res* **2011,** 10, (11),
719   5242-50.
720   55.   Chen, S.; Akter, S.; Kuwahara, K.; Matsushita, Y.; Nakagawa, T.; Konishi, M.; Honda, T.;
721   Yamamoto, S.; Hayashi, T.; Noda, M.; Mizoue, T., Serum amino acid profiles and risk of type 2
722   diabetes among Japanese adults in the Hitachi Health Study. *Sci Rep* **2019,** 9, (1), 7010.
723   56.   Lai, M.; Liu, Y.; Ronnett, G. V.; Wu, A.; Cox, B. J.; Dai, F. F.; Rost, H. L.; Gunderson, E.
724   P.; Wheeler, M. B., Amino acid and lipid metabolism in post-gestational diabetes and
725   progression to type 2 diabetes: A metabolic profiling study. *PLoS Med* **2020,** 17, (5), e1003112.

726   57.   Lu, Y.; Wang, Y.; Liang, X.; Zou, L.; Ong, C. N.; Yuan, J. M.; Koh, W. P.; Pan, A., Serum
727   Amino Acids in Association with Prevalent and Incident Type 2 Diabetes in A Chinese
728   Population. *Metabolites* **2019,** 9, (1).
729   58.   Menni, C.; Fauman, E.; Erte, I.; Perry, J. R.; Kastenmuller, G.; Shin, S. Y.; Petersen, A.
730   K.; Hyde, C.; Psatha, M.; Ward, K. J.; Yuan, W.; Milburn, M.; Palmer, C. N.; Frayling, T. M.;
731   Trimmer, J.; Bell, J. T.; Gieger, C.; Mohney, R. P.; Brosnan, M. J.; Suhre, K.; Soranzo, N.;
732   Spector, T. D., Biomarkers for type 2 diabetes and impaired fasting glucose using a nontargeted
733   metabolomics approach. *Diabetes* **2013,** 62, (12), 4270-6.
734   59.   Wang, T. J.; Larson, M. G.; Vasan, R. S.; Cheng, S.; Rhee, E. P.; McCabe, E.; Lewis, G.
735   D.; Fox, C. S.; Jacques, P. F.; Fernandez, C.; O'Donnell, C. J.; Carr, S. A.; Mootha, V. K.;
736   Florez, J. C.; Souza, A.; Melander, O.; Clish, C. B.; Gerszten, R. E., Metabolite profiles and the
737   risk of developing diabetes. *Nat Med* **2011,** 17, (4), 448-53.
738   60.   Koziel, A.; Woyda-Ploszczyca, A.; Kicinska, A.; Jarmuszkiewicz, W., The influence of
739   high glucose on the aerobic metabolism of endothelial EA.hy926 cells. *Pflugers Arch* **2012,** 464,
740   (6), 657-69.
741   61.   Badawy, A. A., Kynurenine Pathway of Tryptophan Metabolism: Regulatory and
742   Functional Aspects. *Int J Tryptophan Res* **2017,** 10, 1178646917691938.
743   62.   Pedersen, E. R.; Tuseth, N.; Eussen, S. J.; Ueland, P. M.; Strand, E.; Svingen, G. F.;
744   Midttun, O.; Meyer, K.; Mellgren, G.; Ulvik, A.; Nordrehaug, J. E.; Nilsen, D. W.; Nygard, O.,
745   Associations of plasma kynurenines with risk of acute myocardial infarction in patients with
746   stable angina pectoris. *Arterioscler Thromb Vasc Biol* **2015,** 35, (2), 455-62.
747   63.   Sulo, G.; Vollset, S. E.; Nygard, O.; Midttun, O.; Ueland, P. M.; Eussen, S. J.; Pedersen,
748   E. R.; Tell, G. S., Neopterin and kynurenine-tryptophan ratio as predictors of coronary events in
749   older adults, the Hordaland Health Study. *Int J Cardiol* **2013,** 168, (2), 1435-40.
750   64.   Polyzos, K. A.; Ketelhuth, D. F., The role of the kynurenine pathway of tryptophan
751   metabolism in cardiovascular disease. An emerging field. *Hamostaseologie* **2015,** 35, (2), 128-
752   36.
753   65.   Aquilano, K.; Baldelli, S.; Ciriolo, M. R., Glutathione: new roles in redox signaling for an
754   old antioxidant. *Front Pharmacol* **2014,** 5, 196.
755   66.   Yuan, W.; Edwards, J. L., Thiol metabolomics of endothelial cells using capillary liquid
756   chromatography mass spectrometry with isotope coded affinity tags. *J Chromatogr A* **2011,**
757   1218, (18), 2561-8.
758   67.   Weidig, P.; McMaster, D.; Bayraktutan, U., High glucose mediates pro-oxidant and
759   antioxidant enzyme activities in coronary endothelial cells. *Diabetes Obes Metab* **2004,** 6, (6),
760   432-41.
761   68.   Felice, F.; Lucchesi, D.; di Stefano, R.; Barsotti, M. C.; Storti, E.; Penno, G.; Balbarini,
762   A.; Del Prato, S.; Pucci, L., Oxidative stress in response to high glucose levels in endothelial
763   cells and in endothelial progenitor cells: evidence for differential glutathione peroxidase-1
764   expression. *Microvasc Res* **2010,** 80, (3), 332-8.
765   69.   Kashiwagi, A.; Asahina, T.; Ikebuchi, M.; Tanaka, Y.; Takagi, Y.; Nishio, Y.; Kikkawa, R.;
766   Shigeta, Y., Abnormal glutathione metabolism and increased cytotoxicity caused by H2O2 in
767   human umbilical vein endothelial cells cultured in high glucose medium. *Diabetologia* **1994,** 37,
768   (3), 264-9.
769   70.   Hanschmann, E. M.; Godoy, J. R.; Berndt, C.; Hudemann, C.; Lillig, C. H., Thioredoxins,
770   glutaredoxins, and peroxiredoxins--molecular mechanisms and health significance: from
771   cofactors to antioxidants to redox signaling. *Antioxid Redox Signal* **2013,** 19, (13), 1539-605.
772   71.   Scocchi, M.; Tossi, A.; Gennaro, R., Proline-rich antimicrobial peptides: converging to a
773   non-lytic mechanism of action. *Cell Mol Life Sci* **2011,** 68, (13), 2317-30.

774   72.   Migliaccio, A.; Castoria, G.; de Falco, A.; Bilancio, A.; Giovannelli, P.; Di Donato, M.;
775   Marino, I.; Yamaguchi, H.; Appella, E.; Auricchio, F., Polyproline and Tat transduction peptides
776   in the study of the rapid actions of steroid receptors. *Steroids* **2012,** 77, (10), 974-8.
777   73.   Radicioni, G.; Stringaro, A.; Molinari, A.; Nocca, G.; Longhi, R.; Pirolli, D.; Scarano, E.;
778   Iavarone, F.; Manconi, B.; Cabras, T.; Messana, I.; Castagnola, M.; Vitali, A., Characterization
779   of the cell penetrating properties of a human salivary proline-rich peptide. *Biochim Biophys Acta*
780   **2015,** 1848, (11 Pt A), 2868-77.
781   74.   Vanhoof, G.; Goossens, F.; De Meester, I.; Hendriks, D.; Scharpe, S., Proline motifs in
782   peptides and their biological processing. *FASEB J* **1995,** 9, (9), 736-44.
783   75.   Colombo, S.; Melo, T.; Martinez-Lopez, M.; Carrasco, M. J.; Domingues, M. R.; Perez-
784   Sala, D.; Domingues, P., Phospholipidome of endothelial cells shows a different adaptation
785   response upon oxidative, glycative and lipoxidative stress. *Sci Rep* **2018,** 8, (1), 12365.
786   76.   De Keyzer, D.; Karabina, S. A.; Wei, W.; Geeraert, B.; Stengel, D.; Marsillach, J.;
787   Camps, J.; Holvoet, P.; Ninio, E., Increased PAFAH and oxidized lipids are associated with
788   inflammation and atherosclerosis in hypercholesterolemic pigs. *Arterioscler Thromb Vasc Biol*
789   **2009,** 29, (12), 2041-6.
790   77.   Tselepis, A. D.; John Chapman, M., Inflammation, bioactive lipids and atherosclerosis:
791   potential roles of a lipoprotein-associated phospholipase A2, platelet activating factor-
792   acetylhydrolase. *Atheroscler Suppl* **2002,** 3, (4), 57-68.
793   78.   Wang, A.; Dennis, E. A., Mammalian lysophospholipases. *Biochim Biophys Acta* **1999,**
794   1439, (1), 1-16.
795   79.   Marco-Ramell, A.; Palau-Rodriguez, M.; Alay, A.; Tulipani, S.; Urpi-Sarda, M.; Sanchez-
796   Pla, A.; Andres-Lacueva, C., Evaluation and comparison of bioinformatic tools for the
797   enrichment analysis of metabolomics data. *BMC Bioinformatics* **2018,** 19, (1), 1.
798   80.   Zhou, X.; Liao, W. J.; Liao, J. M.; Liao, P.; Lu, H., Ribosomal proteins: functions beyond
799   the ribosome. *J Mol Cell Biol* **2015,** 7, (2), 92-104.
800   81.   Goldberg, A. L., Protein degradation and protection against misfolded or damaged
801   proteins. *Nature* **2003,** 426, (6968), 895-9.
802   82.   Vinals, F.; Pouyssegur, J., Confluence of vascular endothelial cells induces cell cycle
803   exit by inhibiting p42/p44 mitogen-activated protein kinase activity. *Mol Cell Biol* **1999,** 19, (4),
804   2763-72.
805   83.   Yu, Y.; Moulton, K. S.; Khan, M. K.; Vineberg, S.; Boye, E.; Davis, V. M.; O'Donnell, P.
806   E.; Bischoff, J.; Milstone, D. S., E-selectin is required for the antiangiogenic activity of
807   endostatin. *Proc Natl Acad Sci U S A* **2004,** 101, (21), 8005-10.
808   84.   Brigstock, D. R., Regulation of angiogenesis and endothelial cell function by connective
809   tissue growth factor (CTGF) and cysteine-rich 61 (CYR61). *Angiogenesis* **2002,** 5, (3), 153-65.
810   85.   Elmasri, H.; Ghelfi, E.; Yu, C. W.; Traphagen, S.; Cernadas, M.; Cao, H.; Shi, G. P.;
811   Plutzky, J.; Sahin, M.; Hotamisligil, G.; Cataltepe, S., Endothelial cell-fatty acid binding protein 4
812   promotes angiogenesis: role of stem cell factor/c-kit pathway. *Angiogenesis* **2012,** 15, (3), 457-
813   68.
814   86.   Quinn, M. T.; Schepetkin, I. A., Role of NADPH oxidase in formation and function of
815   multinucleated giant cells. *J Innate Immun* **2009,** 1, (6), 509-26.
816   87.   Holt, D. J.; Grainger, D. W., Multinucleated giant cells from fibroblast cultures.
817   *Biomaterials* **2011,** 32, (16), 3977-87.
818   88.   Tse, G. M.; Law, B. K.; Chan, K. F.; Mas, T. K., Multinucleated stromal giant cells in
819   mammary phyllodes tumours. *Pathology* **2001,** 33, (2), 153-6.
820   89.   Celton-Morizur, S.; Merlen, G.; Couton, D.; Desdouets, C., Polyploidy and liver
821   proliferation: central role of insulin signaling. *Cell Cycle* **2010,** 9, (3), 460-6.
822

823   **Figure legends**

824

825   **Figure 1. Illustration of the methodology followed in this study.**

826

827   **Figure 2. Simulated diabetes induced changes in the metabolome of bovine coronary**

828   **artery endothelial cells (BCAEC).** (A) Venn diagram of features identified among MZmine and

829   XCMS software (0.01 Da and 1 min retention time, thresholds) on LC-MS^2 datasets. (B) Volcano

830   plot of all quantified metabolites displaying differences in relative abundance (> +/-30% change,

831   <0.05 *p-value* cut-offs) between BCAEC cultured in control (NG) media and simulated diabetes

832   (HG+ HI) for twelve days. Values (dots) represent the HG+HI/NG ratio for all metabolites. Red

833   and blue dots denote downregulated and upregulated metabolites in the HG + HI group vs. NG

834   group, respectively. (C) Principal Component Analysis (PCA) of LC-MS^2 datasets. Data was log

835   transformed without scaling. Shade areas depict the 95% confidence intervals. (C) HeatMap of

836   the top 100 metabolites ranked by t-test. Abbreviations: NG, normal glucose; HG, high glucose;

837   HI, high insulin; QC, quality control.

838

839   **Figure 3. Bovine coronary artery endothelial cells (BCAEC) metabolite molecular network.**

840   (A) Molecular classes (according to Classyfire) of the metabolome identified by the

841   MolNetEnhancer workflow and visualized by Cytoscape version 3.8.2. Each node represents a

842   unique feature and the color of the node denotes the associated chemical class. The thickness of

843   the edge (connectivity) indicates the MS^2 similarity (Cosine score) among features. The *m/z* value

844   of the feature is shown inside the node and is proportional to the size of the node. Three selected

845   clusters or connected features as relevant are shown. (B) Inset of cluster 1 denoting the presence

846   of phosphocholine (PC)-containing lipids. Significant differential abundant features among

847   simulated diabetes (HG+HI) and control (NG) groups are indicated with an asterisk (*p-value*

848   <0.05). (C) Characterization of features in (B) aided by substructure recognition by MSLDA

849   software using MS^1 visualization in www.ms2lda.org. Fragment at *m/z* 184.0725 linked to a PC

850   head group by mzCloud *in silico* prediction (www.mzCloud.org). Abbreviations: M2M, mass2motif;

851   FC, fold change; NG, normal glucose; HG, high glucose; HI, high insulin. Chemical structures

852   were drawn by ChemDraw Professional version 16.0.1.4.

853

854   **Figure 4. Peptide metabolites modulated by simulated diabetes in bovine coronary artery**

855   **endothelial cells (BCAEC).** (A) Cluster 2 retrieved from the main molecular network linked to

856   glutathione and derivatives. The fragments of mass-2-motif (M2M)_453 colored in red are

857 characteristic of a glutathione core and the fragments are shown in red. (B) Features associated

858 with M2M_453 using MS[1] visualization in www.ms2lda.org. (C) Cluster 3 retrieved from the main

859 molecular network linked to phenylalanine-based metabolites. A singular node at *m/z* 487.1548

860 is also shown. The fragments of M2M_59 colored in red are characteristic of a phenylalanine core

861 (Heuristic and Quantum Chemical predictions by www.mzCloud.org). (D) Features associated

862 with M2M_59 using MS[1] visualization in www.ms2lda.org. In GNPS's clusters (A and C), the

863 node's color denotes the chemical class assigned to the cluster. The thickness of the edge

864 (connectivity) indicates the cosine score (MS[2] similarity). The *m/z* value of the feature is shown

865 inside the node and is proportional to the size of the node. Significant differential abundant

866 features among simulated diabetes (HG+HI) and control (NG) groups are indicated with an

867 asterisk (*p-value* <0.05). In MS2LDA's nodes (B and D), the green node represents the M2M and

868 squares indicate individual features. Edges represent connections to M2M. Significant differential

869 abundant features among groups are indicated with an asterisk (*p-value* <0.05). Abbreviations:

870 M2M, mass2motif; FC, fold change; NG, normal glucose; HG, high glucose; HI, high insulin.

871 Chemical structures were drawn by ChemDraw Professional version 16.0.1.4.

872

873 **Figure 5. Simulated diabetes induced changes in the proteome of bovine coronary artery**

874 **endothelial cells (BCAEC).** (A) Principal Component Analysis (PCA) of LC-SWATH-MS[2]

875 datasets. Data was log transformed without scaling. Shade areas depict the 95% confidence

876 intervals. No scaling was used. (B) Volcano plot of all quantified proteins (Quantile normalization)

877 displaying differences in relative abundance (> +/-20% change, <0.05 *p-value* cut-offs) between

878 BCAEC cultured in control (NG) media and simulated diabetes (HG+ HI) for twelve days. Values

879 (dots) represent the HG+HI/NG ratio for all proteins. Red and blue dots denote downregulated

880 and upregulated proteins in the HG + HI group vs. NG group, respectively. (C) HeatMap of the

881 top 50 metabolites ranked by t-test. Protein-Protein interactome (>0.9 confidence) using the list

882 of proteins with increased abundance (D) and reduced abundance (E) in the HG + HI group.

883 Colored circles denote modules or clusters which may represent relevant complexes or functional

884 units. The input proteins are illustrated with a blue shade and the gene ID is also shown. The

885 most representative pathway (containing more input proteins) for all modules is indicated in blue

886 letters. Abbreviations: NG, normal glucose; HG, high glucose; HI, high insulin.

887

888 **Figure 6. 3D Integrative network of the proteomic and metabolomic perturbations caused**

889 **by simulated diabetes in bovine coronary artery endothelial cells (BCAEC)**. Composite

890 protein-metabolite network created by OmicsNet using the up-regulated proteins (red nodes) and

891   metabolites (magenta nodes) in the HG + HI group (simulated diabetes). Interacting proteins (<0.9

892   confidence) were retrieved from STRING Database and are shown as gray nodes. Abbreviations:

893   NG, normal glucose; HG, high glucose; HI, high insulin.

894

895   **Figure 7. Increased cellular binucleation by simulated diabetes in bovine coronary artery**

896   **endothelial cells (BCAEC) and human coronary artery endothelial cells (HCAEC).** (A)

897   Representative immunofluorescence micrographs showing the localization of the von-Willebrand

898   factor (vWf, 1:400, 3% BSA in PBS) in fixed and permeabilized cells. The nuclei were stained

899   using the dye Hoechst 33258 (2 μg/ml in HBSS). White arrows indicate binucleated cells. (B)

900   Quantification of binucleated cells in HCAEC and BCAEC under simulated diabetes (HG+HI) vs.

901   control (NG) group. Fluorescence images were taken in at least three random fields per condition

902   using an EVOS® FLoid® Cell Imaging Station with a fixed 20x air objective. Image analysis was

903   performed by ImageJ software (version 2.0.0). Abbreviations: NG, normal glucose; HG, high

904   glucose; HI, high insulin.

905

906   **Figure 8. Summary illustration of study findings.** Cellular structures were created using

907   Servier Medical Art templates, which are licensed under a Creative Commons Attribution 3.0

908   Unported License; https://smart.servier.com. Chemical structures were drawn by ChemDraw

909   Professional version 16.0.1.4.

910

911

912

Supporting information

Table S1. List of all the putatively annotated metabolites by MS^2 spectral matching against GNPS public spectral libraries.

Table S2. List of putatively annotated (MS^2 spectral matching) metabolites modulated by simulated diabetes.

Table S3. List of all detected peptides by ProteinPilot Software using the metabolomics datasets.

Table S4 Putative annotated proline-peptides altered by simulated diabetes in Bovine Coronary Artery Endothelial Cells by ProteinPilot Software and manual inspection.

Table S5. List of the detected peptides and proteins in all conditions for SWATH-based quantification.

Figure S1. Proteomics data normalization results using NormalyzerDE. (A) Total intensity of raw data before normalization. (B) Quantitative parameters of normalization algorithms (pooled intragroup coefficient of variation [PCV], median absolute deviation [PMAD], estimate of variance [PEV]). Qualitative parameters of normalization algorithms; (C) Box plots (D) MA plots, and (E) Density plots.

Figure S2. Cellular confluence in control and experimental group. Representative micrographs of Bovine Coronary Artery Endothelial Cells (BCAEC) cultured for 9 days with 5.5 mmol/L glucose (control group) and 20 mmol/L glucose+100 nmol/L insulin (simulated diabetes or experimental group). Images were taken using an EVOS® FLoid® Cell Imaging Station with a fixed 20x air objective. Abbreviations: NG, normal glucose; HG, high glucose; HI, high insulin.
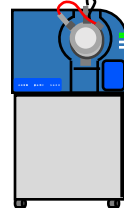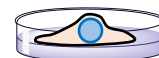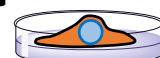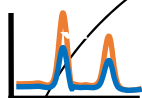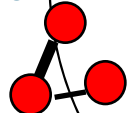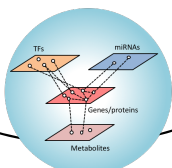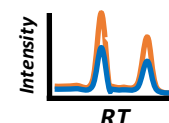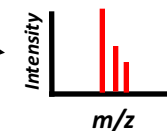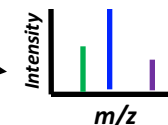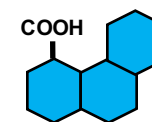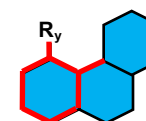
A Total features
detected: 5571

2420
(43.44%)

957
(17.18%)

2194
(39.96%)

B

-Log10 p-value

n=140   n=82

Log2 Fold Change
(HG+HI versus NG)

C

Scores Plot

PC2

PC1

NG
HG+HI
QC

D

Normalized metabolite abundance

NG
HG+HI
QC
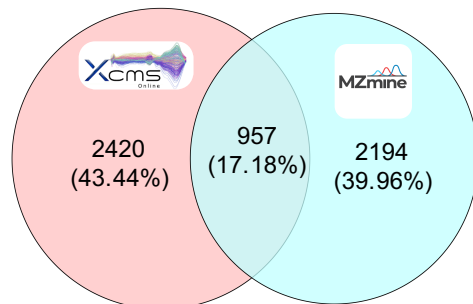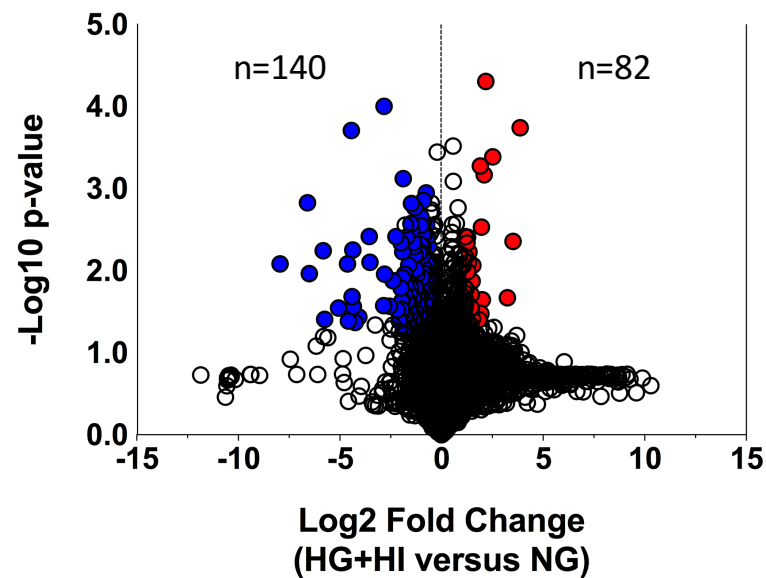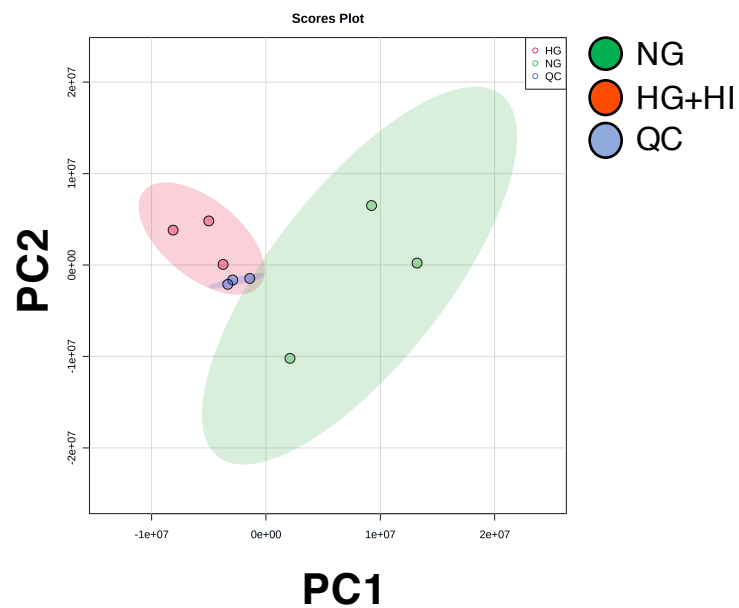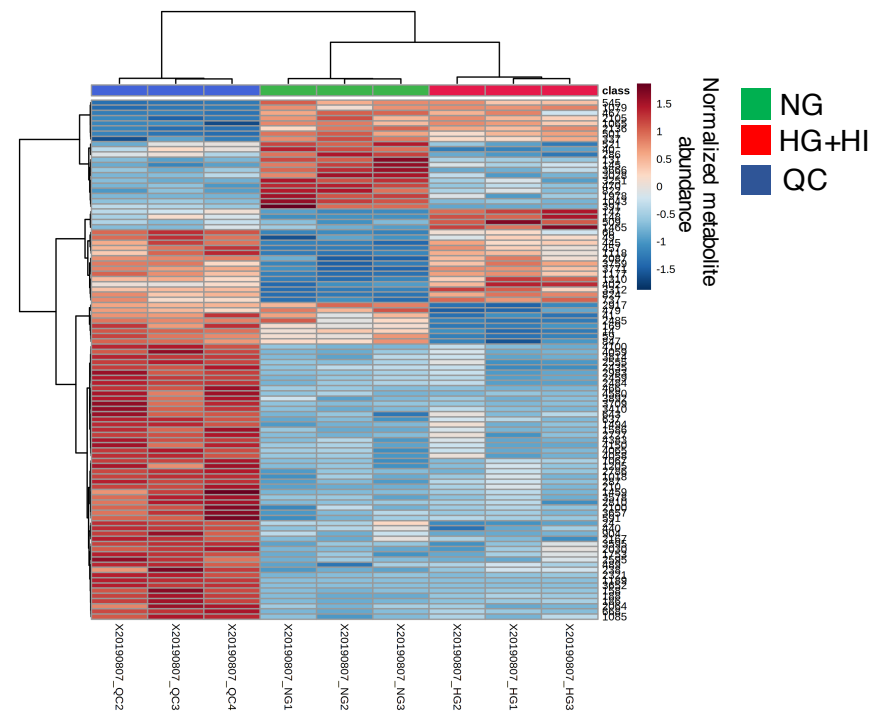
class

A — Chemical class

- Carboxylic acids and derivative
- Glycerophospholipids
- Organooxygen compounds
- Fatty acyls
- Benzene and substituted deriva
- Indoles and derivatives
- Organonitrogen compounds
- Steroids and derivatives
- Coumarins and derivatives
- Glycerolipids
- Unknown

Connectivity (Cosine Score)

Precursor ion *m/z* value

Cluster 1

Cluster 2

Cluster 3

B — Cluster 1

701.5589
703.5731
522.355
786.5972 *
760.5815 *
675.5421
522.3415

PC(16:0/18:1(9Z))

PC(18:0/18:2(9Z,12Z))
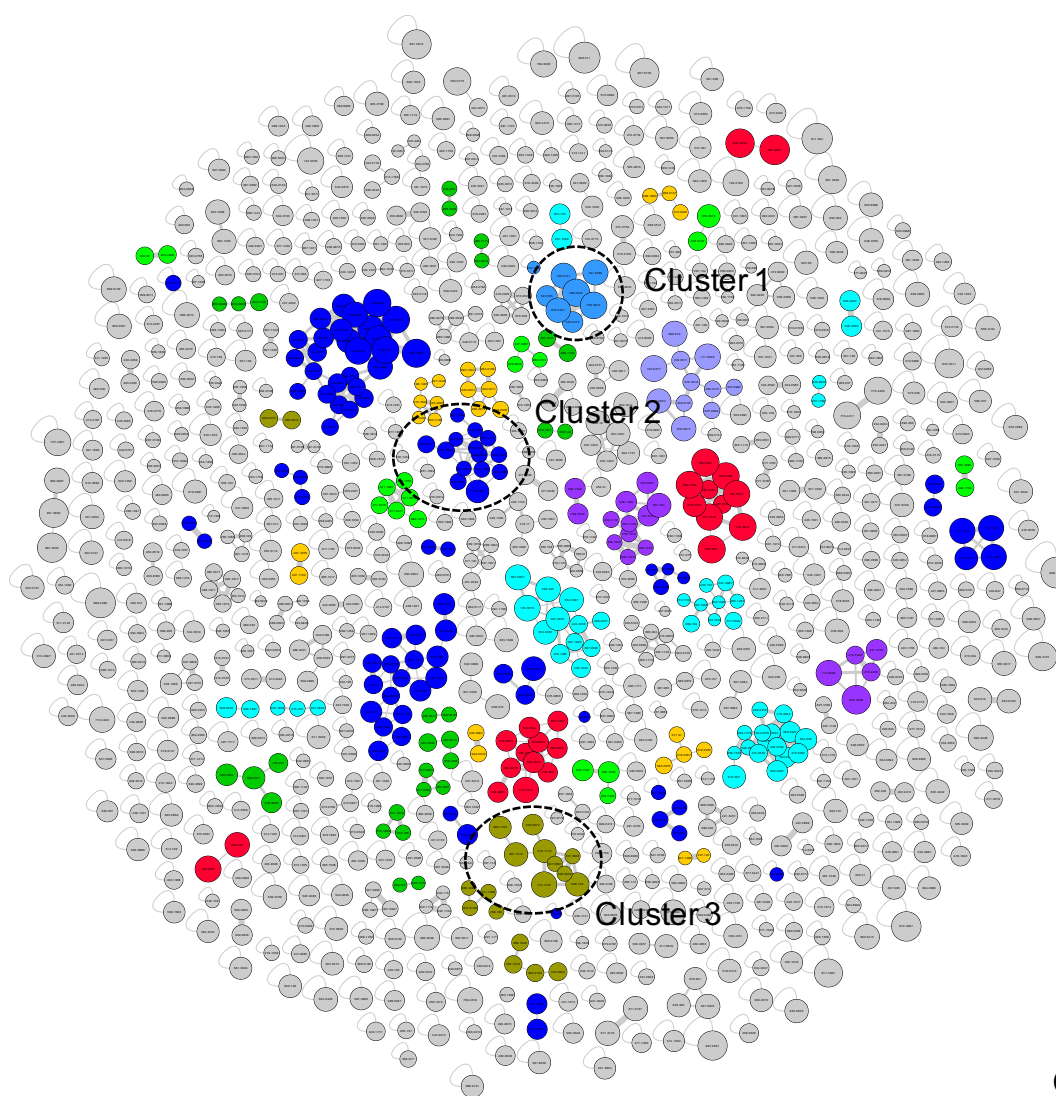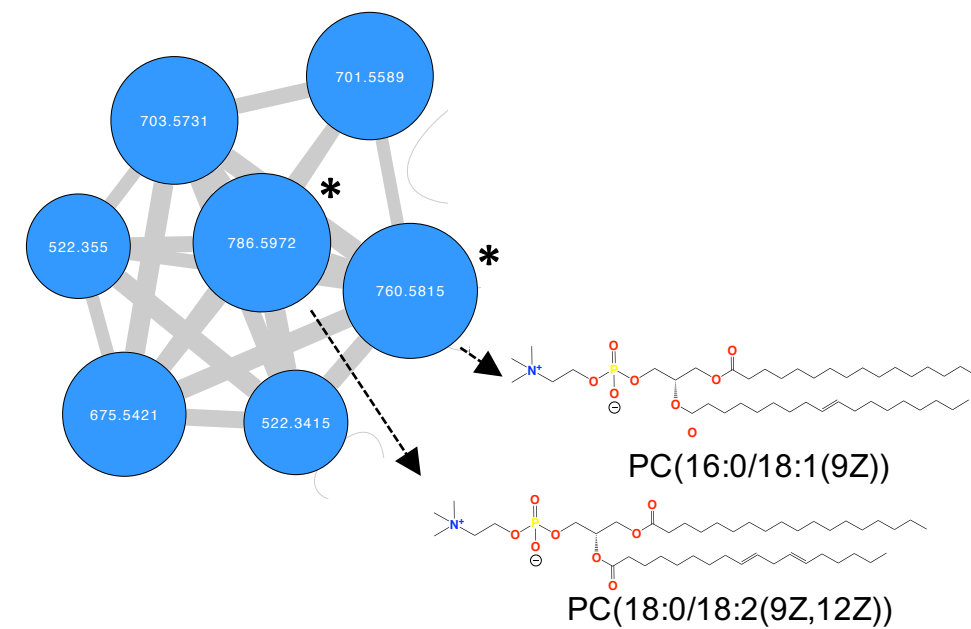
C — MS2LDA

M2M_526_Phosphocholine-based substructure

Log2 FC
3.6
1
-2.6

760.5815
m/z

184.0725

Relative Intensity
100
75
50
25
0
0 100 200 300 400
m/z
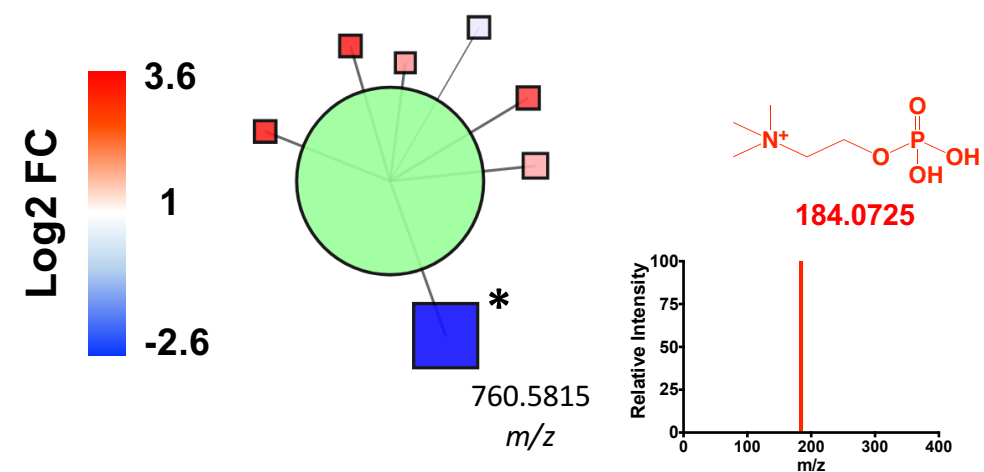
Peptide metabolites

A
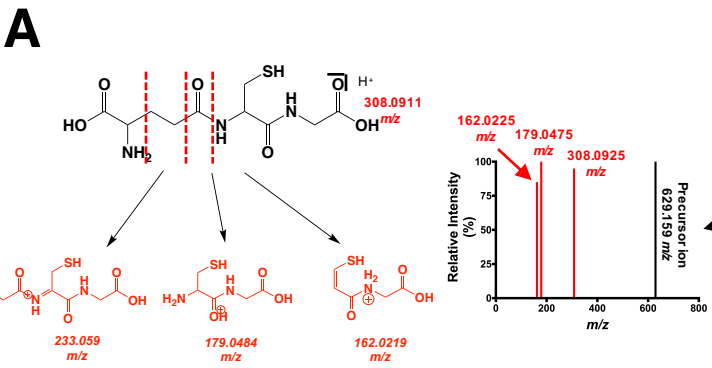
B MS2LDA

M2M_453_Glutathione-based substructure
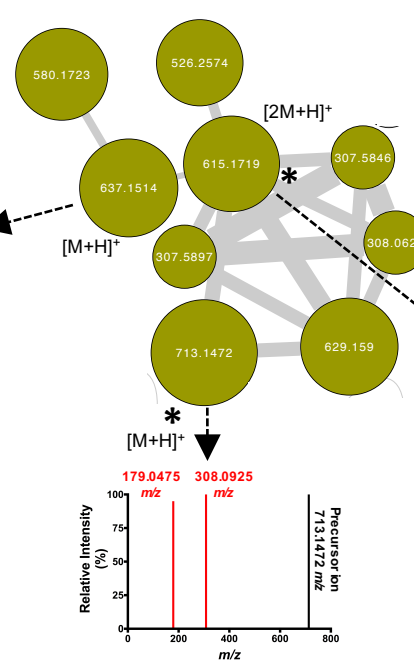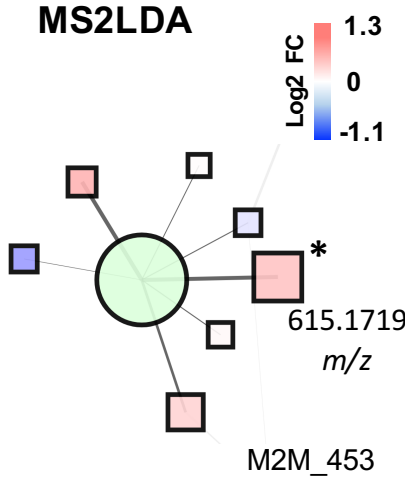
C
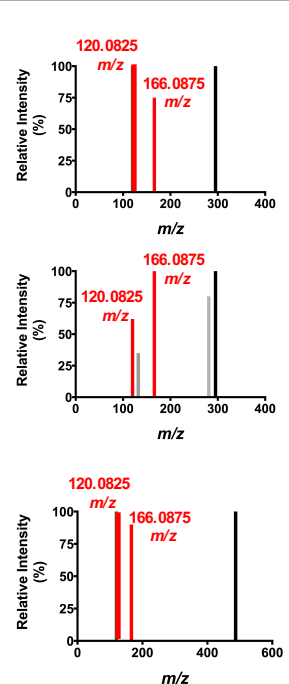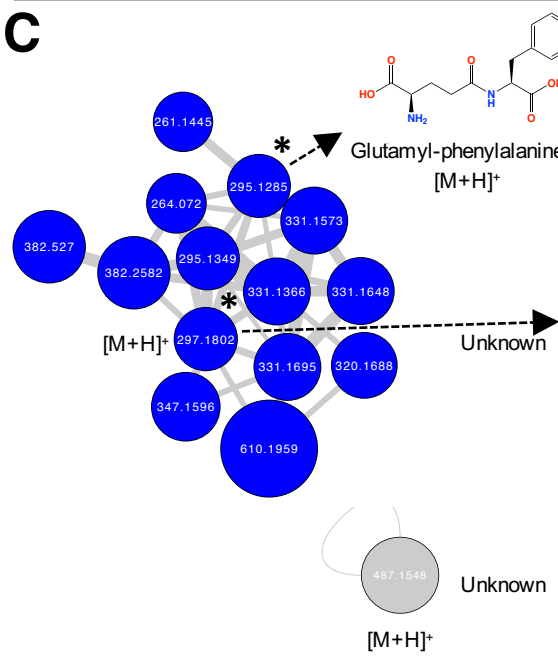
M2M_59_Phenylalanine-based substructure
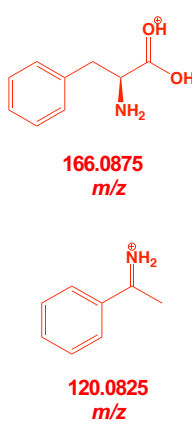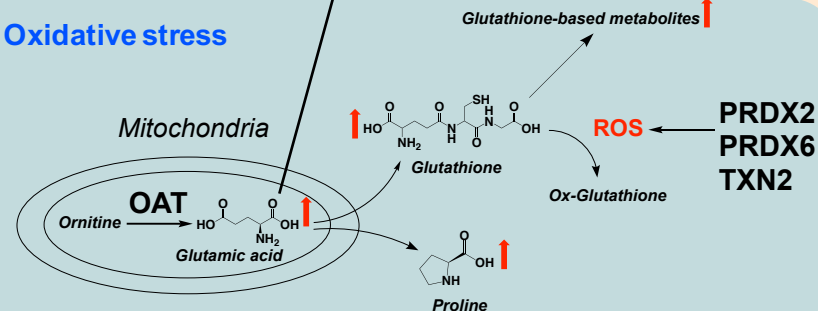
D MS2LDA
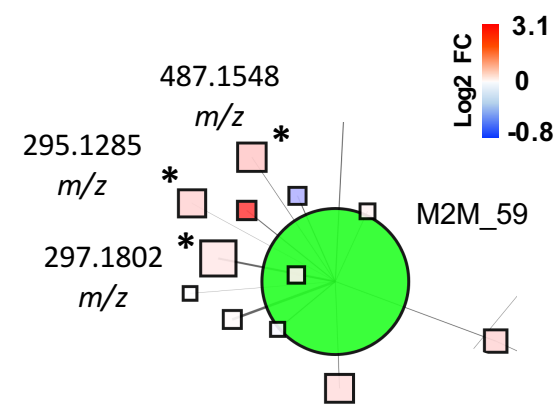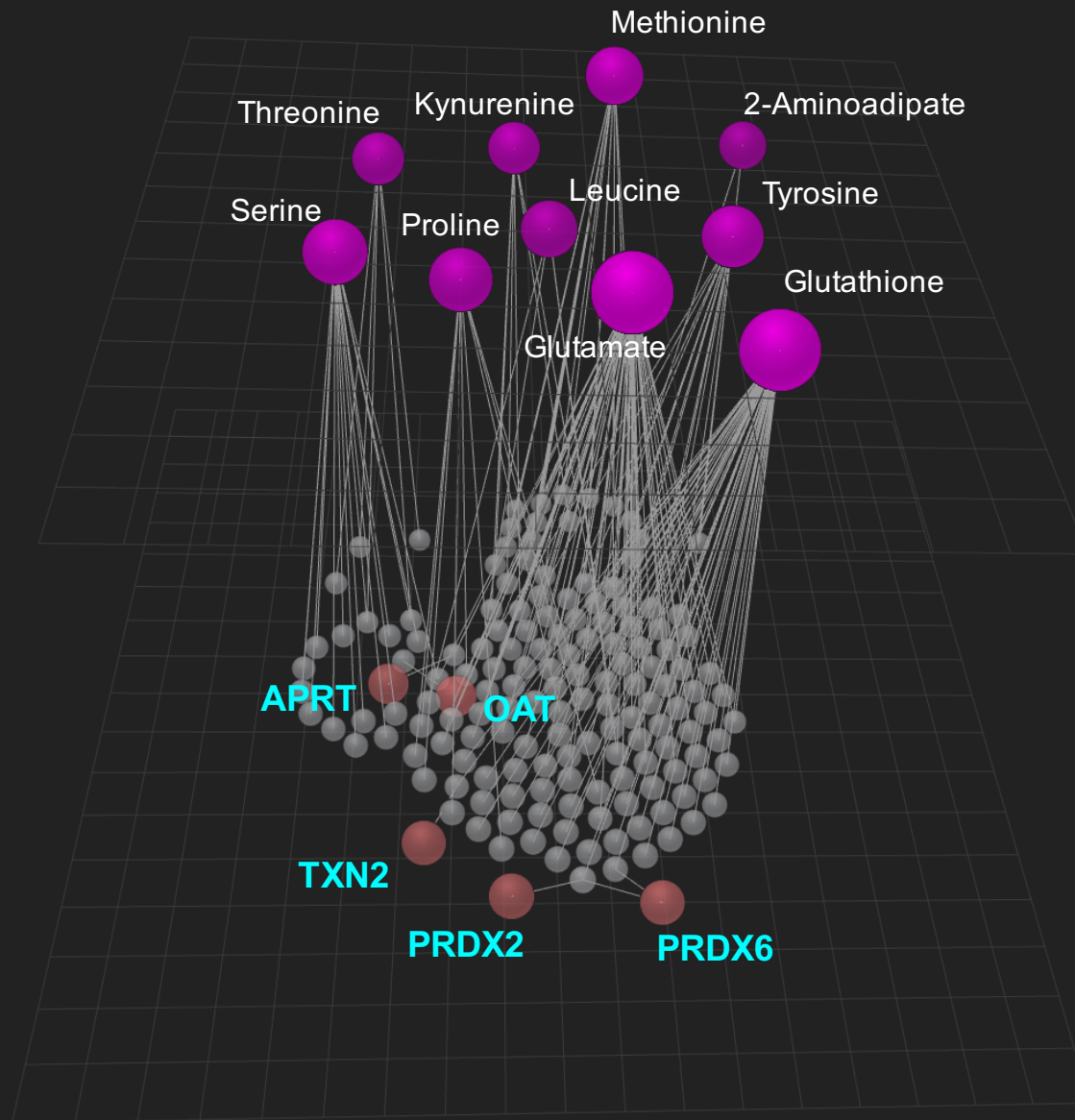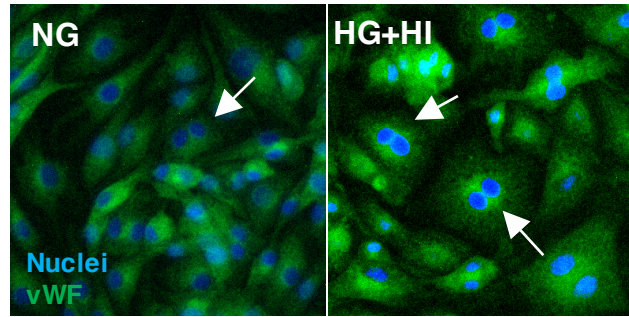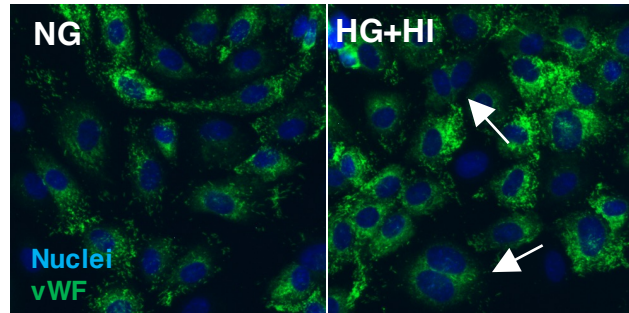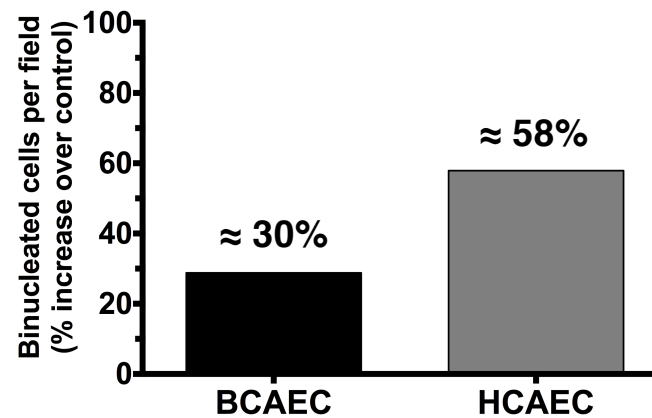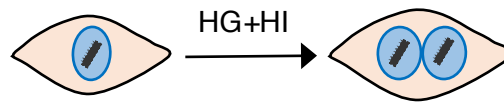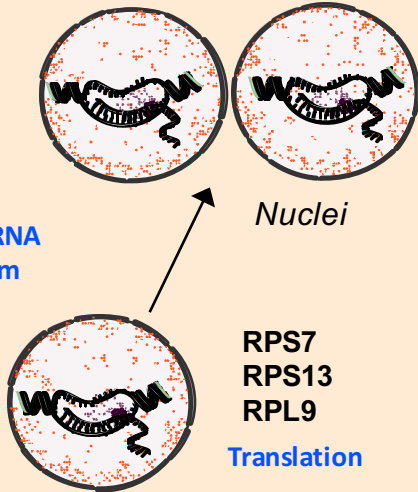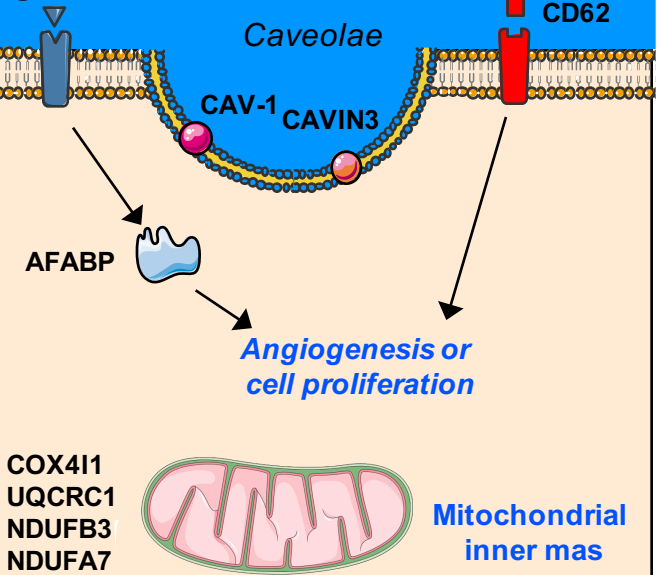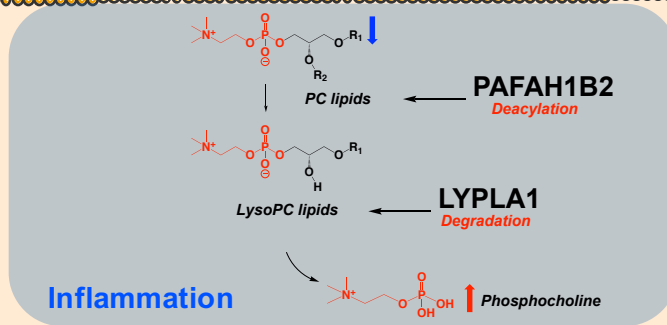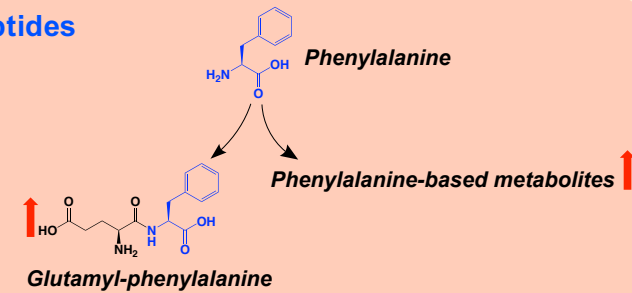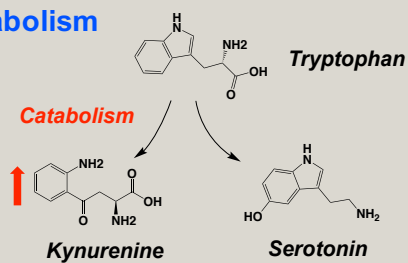
Table 1. Pathway enrichment analysis of up-regulated and down-regulated proteins in HG+HI group

REACTOME Database	Total	Hits	FDR		Total	Hits	FDR
Up-regulated				*Down-regulated*			
Metabolism of RNA	339	142	1.26E-100	Peptide chain elongation	178	77	5.81E-48
Metabolism of mRNA	317	136	1.04E-97	Influenza Infection	185	78	6.52E-48
Synthesis of DNA	95	75	2.37E-79	Nonsense Mediated Decay Independent of the Exon Junction Complex	184	77	4.04E-47
DNA Replication	102	77	5.67E-79	Influenza Life Cycle	180	76	4.63E-47
DNA Replication Pre-Initiation	80	68	3.49E-76	Eukaryotic Translation Elongation	186	77	4.63E-47
M/G1 Transition	80	68	3.49E-76	Nonsense Mediated Decay Enhanced by the Exon Junction Complex	203	80	4.63E-47
S Phase	122	78	4.62E-71	Nonsense-Mediated Decay	203	80	4.63E-47
G1/S Transition	113	75	4.37E-70	Influenza Viral RNA Transcription and Replication	176	75	5.77E-47
Assembly of the pre-replicative complex	63	57	5.61E-67	Viral mRNA Translation	176	75	5.77E-47
Metabolism of RNA	339	142	1.26E-100	Eukaryotic Translation Termination	178	75	1.42E-46
KEGG Database							
Up-regulated				**Down-regulated**			
Basal transcription factors	153	111	2.17E-115	Basal transcription factors	153	88	8.15E-73
Mismatch repair	45	43	1.68E-53	Nucleotide excision repair	135	46	3.62E-24
SNARE interactions in vesicular transport	124	41	2.28E-22	Renal cell carcinoma	201	46	2.26E-16
Base excision repair	36	18	3.46E-13	Endometrial cancer	204	45	1.88E-15
Human papillomavirus infection	155	34	1.62E-12	Peroxisome	137	35	5.32E-14
Chemical carcinogenesis	201	36	1.50E-10	Nicotine addiction	193	41	1.48E-13
Hepatocellular carcinoma	76	18	4.74E-07	Ribosome biogenesis in eukaryotes	79	26	2.92E-13
Human T-cell leukemia virus 1 infection	162	26	1.49E-06	Gap junction	199	41	3.40E-13
Chronic myeloid leukemia	97	19	3.79E-06	Herpes simplex virus 1 infection	225	42	5.11E-12
Notch signaling pathway	160	25	3.79E-06	Glutamatergic synapse	231	36	1.02E-14

Table *2*. Integrative pathway enrichment analysis of up-regulated proteins and metabolites in HG+HI group

REACTOME Database	Total	Hits	FDR	KEGG Database	Total	Hits	FDR
Metabolism of amino acids and derivatives	190	44	8.74E-39	EGFR tyrosine kinase inhibitor resistance	1490	129	1.01E-72
Metabolism	1490	85	1.33E-35	Glutathione metabolism	56	39	1.63E-54
Glutathione conjugation	25	21	7.33E-33	Alanine, aspartate and glutamate metabolism	36	24	4.57E-32
Phase II conjugation	74	25	2.04E-25	ABC transporters	75	27	1.09E-26
Amino acid synthesis and interconversion (transamination)	18	15	5.97E-23	Cysteine and methionine metabolism	49	22	3.48E-24
Biological oxidations	142	25	7.73E-18	Pancreatic cancer	82	23	7.55E-20
tRNA Aminoacylation	42	13	5.19E-12	Drug metabolism - cytochrome P450	72	21	1.67E-18
Glutathione synthesis and recycling	10	7	3.67E-09	Metabolism of xenobiotics by cytochrome P450	76	21	5.18E-18
Sulfur amino acid metabolism	25	9	9.84E-09	Drug metabolism - other enzymes	79	20	2.45E-16
Tryptophan catabolism	11	6	7.51E-07	mRNA surveillance pathway	73	19	8.78E-16